# NOVEL PSO-GA COMPLEX NONLINEAR OPTIMIZATION OF HYBRID RENEWABLE ENERGY SYSTEMS: PV-WIND-PTC INTEGRATION WITH ENERGY STORAGE SYSTEMS

A THESIS SUBMITTED TO
THE GRADUATE SCHOOL OF NATURAL AND APPLIED SCIENCES
OF
MIDDLE EAST TECHNICAL UNIVERSITY

BY
ZAHRA MEDGHALCHI

IN PARTIAL FULFILLMENT OF THE REQUIREMENTS
FOR
THE DEGREE OF MASTER OF SCIENCE
IN
MECHANICAL ENGINEERING

JUNE 2024

Approval of the thesis:

**Novel PSO-GA Complex Nonlinear Optimization of Hybrid Renewable Energy Systems: PV-Wind-PTC Integration with Energy Storage Systems**

submitted by **ZAHRA MEDGHALCHI** in partial fulfillment of the requirements for the degree of **Master of Science** in **Mechanical Engineering**, Middle East Technical University by,

Prof. Dr. Naci Emre Altun
Dean, Graduate School of **Natural and Applied Sciences** ________________

Prof. Dr. Sahir Arıkan
Head of the Department, **Mechanical Engineering** ________________

Assoc. Prof. Dr. Onur Taylan
Supervisor, **Mechanical Engineering, METU** ________________

**Examining Committee Members:**

Prof. Dr. Derek Keith Baker
Mechanical Engineering, METU ________________

Assoc. Prof. Dr. Onur Taylan
Mechanical Engineering, METU ________________

Prof. Dr. Almıla Güvenç Yazıcıoğlu
Mechanical Engineering, METU ________________

Assist. Prof. Dr. Altuğ Özçelıkkale
Mechanical Engineering, METU ________________

Prof. Dr. Murat Köksal
Mechanical Engineering, Hacettepe University ________________

Date: 26.06.2024

**I hereby declare that all information in this document has been obtained and presented in accordance with academic rules and ethical conduct. I also declare that, as required by these rules and conduct, I have fully cited and referenced all material and results that are not original to this work.**

Name, Last name: Zahra Medghalchi

Signature:

# ABSTRACT

## NOVEL PSO-GA COMPLEX NONLINEAR OPTIMIZATION OF HYBRID RENEWABLE ENERGY SYSTEMS: PV-WIND-PTC INTEGRATION WITH ENERGY STORAGE SYSTEMS

Medghalchi, Zahra
Master of Science, Mechanical Engineering
Supervisor: Assoc. Prof. Dr. Onur Taylan

June 2024, 89 pages

Over recent years, there has been a notable surge in the adoption of renewable energy sources, driven by mounting concerns surrounding climate change and the finite nature of fossil fuel resources. In this study, the photovoltaic (PV) system is examined in integration with various Energy Storage Systems (ESS), including batteries and fuel cells. Additionally, it is assessed in hybrid systems that incorporate wind turbines and parabolic trough collector (PTC) systems (integrated with Thermal Energy Storage (TES) and Organic Rankine Cycle (ORC)) for electricity production. The primary objective is to minimize the weighted average cost of energy (waCOE) while ensuring a specific renewable energy fraction ($F_{RES}$). To achieve this, a novel hybrid optimization system utilizing Particle Swarm Optimization (PSO) and Genetic Algorithm (GA) is employed to optimize the capacities of all system components, including the PV panels, wind turbine, battery, electrolyzer, hydrogen tank, fuel cell, trough collector, TES, turbine, evaporator, heat exchangers, condenser, and pump. Additionally, this work optimizes the flow rates of the heat transfer fluid and working fluid under realistic operating conditions, considering the fluctuating efficiency of the ORC and the impact of partial load on turbine efficiency, thus presenting a complex and nonlinear optimization problem. Eight scenarios representing different integrated systems are investigated and compared both technically and economically. A case study is conducted on a university campus located on a Mediterranean island, which relies on imported fossil fuel for electricity production. The findings reveal that a PV-PTC-ORC-TES hybrid system comprising a $14 \times 38$ Trough collector, a $1.76\ MW$ PV, a $121.53\ kWh$ heat storage, and an $774.65\ kW$ ORC has the lowest waCOE at $0.2378\ €/kWh$. This system achieves a demand-supply fraction (DSF) of $57.18\%$ with an $F_{RES}$ of $82.00\%$. The study concludes that a hybrid system incorporating PV and PTC/ORC is highly effective in the examined region due to the abundant solar energy available.

Keywords: Parabolic Trough Collector, Organic Rankine Cycle, Hybrid PV & Wind Systems, Hybrid PSO & GA Optimization, Battery & Electrolyzer-Fuel Cell

# ÖZ

## HİBRİT YENİLENEBİLİR ENERJİ SİSTEMLERİNİN YENİLİKÇİ PSO-GA KARMAŞIK DOĞRUSAL OLMAYAN OPTİMİZASYONU: ENERJİ DEPOLAMA SİSTEMLERİ İLE PV-RÜZGAR-PTC ENTEGRASYONU

Medghalchi, Zahra
Yüksek Lisans, Makina Mühendisliği
Tez Yöneticisi: Doç. Dr. Onur Taylan

Haziran 2024, 89 sayfa

Son yıllarda, iklim değişikliği ve fosil yakıt kaynaklarının sınırlı olmasıyla ilgili artan endişeler nedeniyle yenilenebilir enerji kaynaklarının benimsenmesinde belirgin bir artış olmuştur. Bu çalışmada, fotovoltaik (PV) sistemin, piller ve yakıt hücreleri dahil olmak üzere çeşitli Enerji Depolama Sistemleri (EES) ile entegrasyonu incelenmiştir. Ayrıca, elektrik üretimi için rüzgar türbinleri ve parabolik oluk kollektör (PTC) sistemlerini (Termal Enerji Depolama (TES) ve Organik Rankine Çevrimi (ORC) ile entegre) içeren hibrit sistemlerde değerlendirilmiştir. Ana hedef, belirli bir yenilenebilir enerji oranını ($F_{RES}$) sağlarken ağırlıklı ortalama enerji maliyetini (waCOE) minimize etmektir. Bu hedefe ulaşmak için, PV panelleri, rüzgar türbini, batarya, elektrolizör, hidrojen tankı, yakıt hücresi, oluk kollektör, TES, türbin, evaporatör, eşanjörler, kondenser ve pompa dahil olmak üzere tüm sistem bileşenlerinin kapasitelerini optimize etmek amacıyla Parçacık Sürü Optimizasyonu (PSO) ve Genetik Algoritma (GA) kullanan yenilikçi bir hibrit optimizasyon sistemi kullanılmaktadır. Ayrıca, bu çalışma, ORC'nin değişken verimliliğini ve kısmi yükün türbin verimliliği üzerindeki etkisini göz önünde bulundurarak, gerçekçi çalışma koşulları altında ısı transfer akışkanının ve çalışma akışkanının akış hızlarını optimize eder, böylece karmaşık ve doğrusal olmayan bir optimizasyon problemi sunar. Farklı entegre sistemleri temsil eden sekiz senaryo teknik ve ekonomik olarak araştırılıp karşılaştırılmıştır. Akdeniz'de bir adada bulunan ve elektrik üretimi için ithal fosil yakıta bağımlı olan bir üniversite kampüsünde bir vaka çalışması gerçekleştirilmiştir. Bulgular, 14×38 oluk kollektör, 1.76 MW PV, 121.53 kWh ısı depolama ve 774.65 kW ORC içeren bir PV-PTC-ORC-TES hibrit sisteminin, 0.2378 €/kWh ile en düşük waCOE'ye sahip olduğunu ortaya koymaktadır. Bu sistem, %57.18 talep-karşılama oranı (DSF) ve %82.00 $F_{RES}$ sağlamaktadır. Çalışma, PV ve PTC/ORC içeren bir hibrit sistemin, bol güneş enerjisi nedeniyle incelenen bölgede oldukça etkili olduğunu sonucuna varmıştır.

Anahtar Kelimeler: Parabolik Oluk Toplayıcı, Organik Rankine Çevrimi, Hibrit PV ve Rüzgar Sistemleri, Hibrit PSO ve GA Optimizasyonu, Pil ve Elektrolizör-Yakıt Hücresi

To the courageous women of Iran who strive to bring freedom to the world. With their enduring spirit and unwavering resolve, they embody the essence of "Woman, Life, Freedom".

## ACKNOWLEDGMENTS

I would like to express my heartfelt gratitude to my dear supervisor, Associate Professor Dr. Onur Taylan for his invaluable guidance, support, and encouragement throughout my master's degree. His profound expertise has been instrumental in my growth. I am deeply honored and grateful for his mentorship and unwavering support.

## TABLE OF CONTENTS

# LIST OF TABLES

TABLES

## LIST OF FIGURES

FIGURES

## LIST OF ABBREVIATIONS

| ABBREVIATIONS | |
|---|---|
| ABC | Artificial Bee Colony |
| BESS | Battery Energy Storage System |
| CRES | Combined renewable energy systems |
| CSA | Cuckoo Search Algorithm |
| CSAadaptive-AP | Adaptive Cuckoo Search Algorithm |
| DG | Distributed Generation |
| DHI | Diffuse Horizontal Irradiance |
| DNI | Direct Normal Irradiance |
| DOD | Depth of Discharge |
| EFCS | Eloctrolyser/ Fuel-cell storage |
| ESS | Energy Storage System |
| fmincon | Function Minimization with Constraints |
| fminimax | Function Minimization with Maximum Constraints |
| GA | Genetic Algorithm |
| GHG | Greenhouse Gas |
| GOA | Grasshopper optimization algorithm |
| HDKR | Hay, Davies, Klucher and Reindl mode |
| HOMER | Hybrid Optimization of Multiple Energy Resources |
| HTF | Heat Transfer Fluid |
| LCOE | Levelized Cost of Electricity |
| LPSP | Loss of Power Supply Probability |
| METU NCC | Middle East Technical University Northern Cyprus Campus |
| NOCT | Nominal Operating Cell Temperature |
| NPC | Net present cost |
| NSGAII | Non-Dominated Sorting Genetic Algorithm II |
| ORC | Organic Rankine Cycle |
| PSO | Particle Swarm Optimization |
| PTC | Parabolic trough Collector |
| PV | Photovoltaic |
| RES | Renewable Energy Systems |
| TAC | Total Annual Cost |
| TMY | Typical Meteorological Year |

# LIST OF SYMBOLS

SYMBOLS

| | |
|---|---|
| $A_M$ | Module area, $m^2$ |
| $A_a$ | Aperture Area, $m^2$ |
| $C_{B,i}$ | Capacity of the battery at a particular time "i", kWh |
| $C_{max,B}$ | Maximum capacity of the battery, kWh |
| $C_{H,i}$ | Amount of hydrogen that is in the tank at a particular time "i", kWh |
| $C_{H,tank}$ | Capacity of hydrogen tank, kWh |
| $C_i$ | Initial capital cost, € |
| $C_{p,ave}$ | Average Specific Heat Capacity Coefficient, $\frac{J}{kg.K}$ |
| CosE | Cost of self-consumed produced electricity, €/kWh |
| D | Energy demand, kWh |
| DSF | Yearly Demand-Supply Fraction, % |
| $E_{PV}$ | Energy generated by a PV system, kWh |
| $F_{RES}$ | Yearly renewable energy fraction, % |
| $G_{NOCT}$ | Reference irradiance at nominal conditions, $W/m^2$ |
| $G_T$ | Total irradiance on a tilted surface, kW |
| H | Yearly number of hours which the energy system covered the demand, hr |
| $I_T$ | Incident total radiation on the tilted surface, kWh |
| k | Weibull distribution shape parameter of the wind speeds |
| l | Lifetime, year |
| $M_t$ | Annual operation and maintenance costs, €/kW |
| $M_{Cst}$ | Stored HTF in the Cold Tank, $kg$ |
| $M_{Hst}$ | Stored HTF in the Hot Tank, $kg$ |
| $\dot{m}_{PTC}$ | Flow Rate Heated by the PTC System |
| $N_L$ | Number Of Loops |
| $N_C$ | Number Of Collectors |
| $N_M$ | Number of modules |
| P | Temporary memory for the power, kW |
| $P_{Def}$ | Deficit energy, kWh |
| $P_e$ | Average energy generated from the wind turbine, kWh |
| $P_{EL}$ | Electrolyser power, kW |
| $P_{FC}$ | Fuel cell power, kW |
| $P_{gen}$ | Generated energy by renewable system, kWh |
| $P_{Grid,i}$ | Energy supplied by grid at particular time "i", kWh |
| $P_{Grid}$ | Energy supplied by grid, kWh |

| | |
|---|---|
| $P_{inj,i}$ | Injected energy to the system at particular time "i", kWh |
| $P_{Load}$ | Load, kWh |
| $P_{mpp}$ | Module nominal output, kW |
| $P_{Net}$ | Difference between generated energy and load, kWh |
| $P_P$ | Cycle pump, kW |
| $P_{P,cond.}$ | Condenser pump, kW |
| $P_{rated}$ | Wind turbine rated power, MW |
| $P_T$ | Turbine output power, kW |
| $P_{RES}$ | Demand covered by the RES, kWh |
| $P_{Res,i}$ | Energy supplied by renewable system at particular time "i", kWh |
| $\dot{Q}_{u,PTC}$ | Useful energy output of the PTC system, kW |
| $\dot{Q}_{evap}$ | Heat flux in evaporator, kW |
| r | Discount rate, % |
| t | Time, year |
| $T_{a\ NOCT}$ | Reference ambient temperature at nominal conditions, °C |
| $T_{amb}$ | Ambient temperature, °C |
| $T_{Cst}$ | Cold storage temperature |
| $T_{Hst}$ | Hot storage temperature |
| $T_{HTF,avg}$ | Average HTF temperature |
| $T_{PV}$ | Module temperature, °C |
| $T_{STC}$ | PV cell temperature at standard test conditions, °C |
| $\bar{u}$ | Average wind speed at hub height, m/s |
| $u_{cut-in}$ | Cut-in speed of the wind turbine, m/s |
| $u_{cut-out}$ | Cut-out speed of the wind turbine, m/s |
| $u_g$ | Wind speed at reference level, m/s |
| $u_{rated}$ | Rated speed of the wind turbine, m/s |
| $u_Z$ | Wind speed at hub elevation, m/s |
| waCOE | Weighted-average cost of electricity, €/kWh |
| Z | Height of the wind turbine hub, m |
| $Z_g$ | Height of the reference level, m |
| **Greek letters** | |
| α | Shear coefficient |
| $\beta_{ref}$ | Temperature coefficient of PV for power, % $K^{-1}$ |
| $\Delta T_f$ | temperature difference between the average HTF temperature and the ambient temperature, °C |
| Σ | Wind speeds standard deviation, m/s |

| | |
|---|---|
| $\eta_{charge}$ | Charge efficiency, % |
| $\eta_{EL}$ | Efficiency of electrolyser, % |
| $\eta_{FC}$ | Efficiency of fuel cell, % |
| $\eta_{I}$ | Photovoltaic system losses, % |
| $\eta_{ORC}$ | ORC efficiency, % |
| $\eta_{PV}$ | PV module's efficiency, % |
| $\eta_{PV,ref}$ | PV module reference efficiency, % |
| $\eta_{PTC}$ | Collector's Efficiency, % |

# CHAPTER 1

# INTRODUCTION

## 1.1 Background

Over recent years, there has been a notable surge in the adoption of renewable energy sources, driven by mounting concerns surrounding climate change and the finite nature of fossil fuel resources. Renewable Energy Systems (RES) integrated into existing grids have emerged as a viable solution to meet the escalating global demand for electricity while concurrently mitigating greenhouse gas emissions. Among these alternatives, solar energy stands out as a particularly promising option due to its status as a clean and abundant renewable resource available in most regions [1].

The sun radiates an immense amount of energy to the earth, with just 90 minutes of sunlight delivering enough energy to satisfy the planet's entire annual energy needs [2]. This abundance is staggering, as it theoretically surpasses the projected energy consumption of the global population in 2035 by a factor of 4200. In just a few hours, the Earth receives enough solar energy to cover its entire annual energy consumption [3]. Consequently, harnessing solar energy offers a compelling strategy to curtail carbon emissions. For instance, in California, USA, the installation of solar systems on approximately 113,533 households has resulted in a significant reduction of approximately 696,544 metric tons of carbon emissions [4]. Beyond its environmental benefits, solar energy offers economic advantages, including its long-term cost-effectiveness and versatility, which have garnered considerable attention as a promising alternative to fossil fuels.

Despite its promise, challenges persist in the widespread adoption of solar energy. Issues such as relatively low efficiency, high initial costs, and the need for efficient energy storage solutions pose significant hurdles. However, ongoing technological advancements hold the promise of addressing many of these challenges in the future, ensuring the continued growth and viability of solar energy as a key component of the global energy landscape [2].

Solar energy is harnessed through various methods, including PV systems, which directly convert sunlight into electricity, making them ideal for residential, commercial, and utility-scale applications. Additionally, solar thermal technologies, such as trough collectors, Fresnel reflectors, solar towers, and dish collectors, concentrate sunlight to generate heat for electricity production, water heating, and industrial processes. These technologies offer versatile solutions for meeting energy needs across diverse sectors, ranging from power generation to heating and cooling applications.

In parallel, microgrids have gained significant importance. Microgrids, independent energy systems capable of "islanding" energy production and distribution when the main grid is damaged or unavailable, play a crucial role in ensuring energy reliability, particularly in rural, remote, and areas with unreliable main power grids. Among the various solar energy technologies, mature PV systems and trough collectors stand out as the most suitable options for microgrids. PV systems directly convert sunlight into electricity, making them efficient and versatile for diverse applications. Meanwhile, trough collectors, capable of converting direct solar radiation into thermal energy by heating HTF up to 565℃ [5] are ideal for many commercial applications, including industrial thermal processes and electricity generation via Rankine cycles. Integrating these solar technologies into microgrids not only enhances energy reliability but also provides essential infrastructure, such as hospitals, homes, and schools, with a reliable energy lifeline, ensuring uninterrupted operation even during grid disruptions.

To further enhance the reliability of RES systems, ESS are utilized to balance the intermittency of RES output. Various types of ESSes, including Battery Energy Storage System (BESS) and Electrolyzer-Fuel Cell Storage (EFCS), play critical roles. BESS is a well-established technology for energy storage, while EFCS is a relatively new technology that has gained attention due to its ability to store energy in the form of hydrogen. The integration of RESs with energy storage has gained significant attention in recent years due to their potential to address the challenges of incorporating intermittent renewable energy sources into microgrids.

Another auxiliary force for increasing the feasibility and reliability of RES is using them within a hybrid system. Hybrid systems of renewable energies offer several benefits, including increasing dispatchable renewable energy, improving rural energy access reliability, reducing reliance on fossil fuels, increasing the eco-efficiency of energy production, and lowering long-term energy costs. They can also provide modern energy access to remote areas without the need for expensive transmission and distribution lines from the central grid. Thus, optimal design investigations have been conducted to enhance their effectiveness [6].

Hybrid RESs utilize two or more distinct renewable resources in locations where multiple resources are abundant or have complementary characteristics. For instance, a hybrid system combining solar and wind energy takes advantage of good solar irradiation during the day and wind flow at night. Additionally, a hybrid RES may use the same type of renewable resource if it is particularly abundant in that area. For example, a hybrid system integrating PV and parabolic trough collector (PTC) technology can be employed in regions with high solar energy potential. In both types of hybrid systems, energy storage solutions play a crucial role in mitigating the intermittency of the resources and enhancing the system's autonomy.

The process of creating, improving, and executing hybrid RESs is a challenging task that often necessitates the use of multi-objective techniques to solve it [7]. This complexity arises from the unpredictable variability of input parameters of the energy sources being considered over time and their independence from the energy load requirements [8].

## 1.2 Objectives

This study investigates two types of hybrid renewable energy systems (RESs): one that utilizes multiple renewable resources (wind and solar energy) and another that relies on a single resource (solar energy). Specifically, it explores two hybrid systems: one combining PV panels with a wind turbine, and another integrating PV panels with a parabolic trough collector (PTC) and an organic Rankine cycle (ORC) setup. The selected case study location, the METU NCC university campus in Northern Cyprus, has high solar energy potential complemented by wind energy, making these hybrid systems particularly suitable.

To enhance system autonomy and reliability, energy storage solutions including BESS, EFCSs, and thermal energy storage (TES) are utilized. The sizing of each component is optimized using a novel scheme that minimizes energy costs while maintaining a specific renewable energy fraction.

In the initial phase, the research evaluates the integration of PV panels, wind turbines, and a combined PV-wind system with BESS and EFCS in a grid-connected setup. Subsequently, it assesses the feasibility of the hybrid PV/PTC system and compares it with standalone PV and standalone PTC systems.

A key innovation of this study is the hybrid optimization method combining Particle Swarm Optimization (PSO) and Genetic Algorithm (GA) to determine optimal capacities for all system components, including trough collectors, PV panels, wind turbines, batteries, electrolyzers, hydrogen tanks, fuel cells, thermal storage tanks, turbines, evaporators, heat exchangers, condensers, and pumps. Additionally, it optimizes the flow rates of the heat transfer fluid and working fluid in the PTC/ORC system under realistic operating conditions, considering the fluctuating efficiency of the ORC and the impact of partial load on turbine efficiency.

The comprehensive economic analysis adds depth to the research, demonstrating that this hybrid optimization approach can significantly enhance the contribution of renewable energy sources to microgrid energy demands, providing a reliable and efficient dispatch system. This research paves the way for increased adoption of hybrid renewable systems, ensuring sustainable and dependable energy solutions for microgrids.

## 1.3 Literature Review

This section systematically examines and categorizes existing research to provide a comprehensive understanding of the different components and methodologies related to the study. Various aspects are explored, including PV systems, PTC, wind turbine, and energy storage solutions. Additionally, the integration of these technologies into hybrid RESs and the optimization techniques used to enhance their performance are investigated. Each section critically analyzes state-of-the-art advancements, highlighting key findings, innovations, and gaps in the current body of knowledge.

### 1.3.1 PV

PV technology, a well-established means of harnessing solar energy, has been extensively researched by numerous scholars. These studies explore various aspects of PV systems, including standalone PV systems [9], PV integrated with diverse storage solutions such as batteries and hydrogen [7, 10-13], and hybrid systems combining PV with other renewable sources like wind and hydro [14-16]. The investigations encompass optimization of system size, feasibility assessments, and both technical and economic analyses. For instance, Aziiz et al. [17] conducted a study aiming to analyze the techno-economic and environmental feasibility of a solar PV microgrid system capable of supplying power during grid availability and outages. Utilizing HOMER software, they employed five different control strategies and found the most economical configuration to involve grid charging of batteries at all rates, with a net present cost (NPC) of 29,713 $.

Alramlawi [18] proposed a comprehensive method for optimal design of residential PV-battery microgrids, considering factors such as the optimal number of batteries and PV panels, battery bank depth of discharge (DOD), and PV panel tilt angle, with the goal of minimizing the levelized cost of energy (LCOE) while adhering to operational constraints. Shafiullah et al. [19] evaluates the techno-economic feasibility of PV based systems employing hydrogen as energy storage for off-grid microgrids. Simulation results suggest the hydrogen-battery hybrid ESS as the most cost-effective scenario, while acknowledging the viability of other scenarios with distinct merits and challenges. Furthermore, Yuan et al. [20] explores a PV and energy storage optimization configuration model using the second-generation non-dominated sorting genetic algorithm (NSGA-II), which considers load characteristics, environmental factors, and economic variables. The results demonstrate the effectiveness of the optimized PV and ESS in enhancing PV utilization rates and microgrid system economics.

### 1.3.2 PTC

Another means of harnessing solar energy is Parabolic Trough Collector. PTC, a staple in large-scale power plants, offers a significant avenue for solar energy utilization. Within Concentrating Solar Power (CSP) systems, direct normal solar radiation is captured and transformed into thermal energy, powering a generator to produce electricity. Research delves into various aspects of these systems, exploring factors like working fluids, power block configurations, stability, and economic viability. For instance, Singh et al. [21] examined the effects of different working fluids, observing a notable $11.10\%$ increase in useful heat generation with MXene-based nanofluid compared to Syltherm 800. Despite higher costs, the levelized cost of electricity for the MXene-based system was slightly lower.

In another study [22], Ata et al. compared power cycle performance for PTC, finding the ORC with $R123$ with heat exchanger to be superior in power production and emission reduction, while the Kalina Cycle offered better economic feasibility. The investigation into an automated design of a radial turbine model for a solar ORC coupled to a PTC in [23] revealed significant impacts of turbine operating conditions and design parameters on system performance. For instance, a 100 $kPa$ increase in evaporation pressure led to a 17.5% reduction in turbine size. Similarly, as the turbine pressure ratio increased from 1.5 to 4.5, the efficiency of the PTC decreased by 1.7%, while the efficiency of the ORC surged by 200%.

In the study outlined by Martin et al. [24], a parabolic collector boasting a tube length of 18.12 meters underwent design and manufacturing processes. During a 2-hour test, results indicated that the parabolic trough achieved a temperature of 56.6°C with a water flow rate of 0.042 $kg/s$, up from an initial temperature of $28.2°C$. The theoretical calculations suggested an average turbine output power of 430 $W$, whereas in reality, the ORC system yielded 248.57 $W$. Notably, the highest thermal efficiency was attained at a turbine inlet temperature of $63.5°C$ and inlet pressure of 10.5 bar, registering at 4.489%. These findings underscore the efficacy of ORC technology in harnessing low-level heat sources, thereby aiding in the reduction of reliance on fossil fuels and mitigating thermal pollution.

Desai et al. [25] presents an in-depth energy and economic analysis of a PTC-based CSP plant, specifically focusing on systems without storage. The study explores the effects of turbine inlet pressure, turbine inlet temperature, design radiation, plant size, and different modifications of the Rankine cycle on overall efficiency and LCOE. For an 1 $MWe$ plant utilizing a basic Rankine cycle, optimal turbine inlet pressures are found to be approximately 4.5-7.5 $MPa$ for energy efficiency and $3.5 - 7.5$ $MPa$ for cost efficiency. In another study [26], a simplified model was employed by Cabello et al. to optimize the size of a solar power plant's components for maximum yearly profit. Traditional optimization methods were impractical, leading to the use of GA. Results indicated an optimum collector area ranging between 583,000 $m^2$ and 749,860 $m^2$, with corresponding thermal storage varying from 6.55 to 13.46 hours. Economic benefits consistently exceeded 19.30 $M€$ per year, with electricity production costs averaging around 18.5 $c€/kWh$.

In a separate study, Quoilin et al. [27], the design and performance optimization of a low-cost solar ORC for remote power generation were investigated. The system, designed for rural electrification in Lesotho, comprised PTCs, storage tanks, and small-scale ORC engines. Various working fluids and expansion machine configurations were evaluated for performance and cost-effectiveness.

### 1.3.3 Wind Turbine

Wind energy has risen to prominence as the second most commonly adopted renewable energy source, representing 4% of global electricity generation [28]. A multitude of studies have examined the potential of wind energy. These investigations address different aspects, including methodologies to identify suitable lands [29, 30] and the techno-economic viability of wind farms [31].

Solyali et al. [32] compared the cost of electricity production by wind turbines with solar energy for several locations in Cyprus. They summarized that in the best case, the lowest LCOE of wind energy reaches 0.2 €/kWh whereas the minimum cost of solar energy calculated as 0.127 €/kWh during wind farms life time. Despite wind energy systems exhibiting a significantly higher internal rate of return compared to PV systems in Northern Cyprus, Ilkan et al.[33] noted that in certain locations, wind energy systems yield greater economic benefits. N'guessan et al. [34] focused on minimizing both the total Annual Cost (TAC) and Loss of Power Supply Probability (LPSP) of a wind powerplant integrated with several ESS. Results indicated that using the EES the lowest attained LPSP would be 4.4 percent.

In another study, Fokaides et al.[35] discussed the viability of the Orites wind farm in Southern Cyprus, boasting a capacity of 82 MW. The levelized cost of electricity for this wind farm was recorded at 0.1 €/kWh, while the grid tariff stood at 0.166 €/kWh.

### 1.3.4 Energy Storage

Several studies cited in the literature [36-38] underscore the capacity of ESS to enhance the dependability of Renewable Energy Sources (RESs) and optimize the synchronization of energy supply and demand. This involves harnessing surplus electricity produced by RESs during periods of excess supply to charge the ESS, subsequently discharging stored energy during times of high demand, thereby efficiently mitigating fluctuations in energy supply and demand.

A study by Chico et al.[39] optimized BESS sizing and placement for maximum renewable energy source penetration, considering demand response flexibility and key indicators like technical minimum load and system ramp capacity. Results from the simulated energy system in Indonesia showed significant cost reductions (up to 37.66%) and increased renewable energy source penetration (up to 83%) compared to current system conditions across different scenarios.

Rayit et al. [40] explore replacing gas turbine power plants with wind energy and bulk battery storage in the UK, focusing on techno-economic viability. A model was developed to optimize Li-ion battery sizing for grid-level energy applications, revealing that at a 200 £/kWh battery cost and 15% wind curtailment, a 1.25 GWh battery could meet 285 GWh peak demand annually, yielding a net present value of 22.4 M£, 1.7% internal rate of return, and 14-year payback period. However, achieving an 8% internal rate of return requires battery costs below 150 £/kWh.

Several feasibility studies have delved into the potential of EFCS as large-scale ESS. One notable study by Devrim et al. [41] concentrated on generating electrical power for an average 150 $m^2$ house, proposing a hybrid system incorporating PV and wind turbines integrated with EFCS in Ankara, Turkey. According to the findings, this recommended hybrid system adequately meets demand throughout the year, except for November.

Dong et al.[42] examined various EES systems for wind energy storage, with the lithium-ion battery demonstrating the highest efficiency at 71% for energy and 61.5% for exergy. Conversely, the fuel cell-electrolyzer hybrid system exhibited lower performance. Economically, the fuel cell-electrolyzer hybrid system proved most favorable with a ratio of energy stored to electrical energy invested of about 53, while the lithium-ion battery showed a lower value of 29. Therefore, while lithium-ion batteries are energetically promising for wind energy storage, the fuel cell-electrolyzer hybrid system is economically advantageous.

### 1.3.5 Hybrid Renewable Energies System

The integration of PV systems with CSP technology has emerged as a significant area of interest in solar energy research. This hybrid approach offers distinct advantages over using PV or CSP technologies independently. PV-CSP hybrids are capable of producing electricity with improved power quality compared to standalone PV systems. Moreover, they can achieve lower power generation costs than systems relying solely on CSP technology [43].

A study by Starke et al. [44] in Chile assessed hybrid PTC+PV and Central Receiver System (CRS)+PV systems, optimizing storage and power block sizes using TRNSYS. Optimization focused on minimizing LCOE while ensuring baseload capacity factors. Results indicate that hybridization increased high-capacity solutions, reducing both CSP field size and LCOE. Moreover, hybrid plants operate PV at non-optimal angles to support base-load production during winter. The study in Saudi Arabia [45] investigate PTC standalone and hybrid configurations in three main parts: simulating standalone PTC, integrating PTC with PV for daytime use, and using excess PV energy for thermal storage. Unlike previous studies, a fixed high-capacity factor is maintained, exploring scenarios with low solar multiples for minimum LCOE. The research simulates each plant configuration separately using NREL's SAM software, then integrates technical and economic models to calculate LCOE. Results show that while a standalone CSP plant requires high solar multiples, hybridization substantially reduces that. For Riyadh, solar multiples range from 2.9 to 3 with equal PV and CSP capacities, and 1.78– 1.85 with greater PV capacity. In Tabuk, solar multiples range from 1.95 to 1.6.

Pilotti et al. [46] present a framework for co-optimizing the design and operation of hybrid CSP-PV power plants. It characterizes all system components in SAM and Thermoflex, then linearizes nonlinear models within a MILP formulation for optimization. The problem determines optimal component sizes (solar field, PV, TES, power block) and dispatchability using a clustering algorithm. Results show the hybrid layout's cost advantages ($35.3\%$ $to$ $47.7\%$ lower compared to standalone solutions) and increased reliability and dispatchability. Economic benefits of physical hybridization (using excess PV for thermal storage via electric heater) are also explored, reducing electricity costs by $3.6-10\%$ depending on desired dispatchability.

Aguilar et al. [43] conducts an economic and technical analysis of a hybrid PV-CSP system for use in isolated microgrids, using Puertecitos, Baja California, Mexico as a case study. The system comprises solar concentrators with thermal storage activating a 30 kW ORC to meet energy demand during low solar radiation periods. A PV field supplies $73\ kW$ during daytime, while CSP stores heat for later use. Results indicate the hybrid system's LCOE is only 2% higher than PV-Battery, at $0.524\ \$/kWh$. Scaling up energy demand yields lower LCOE, with a $26\%$ reduction for demand exceeding 500 kW. Fully utilizing the system's capacity throughout the year makes its LCOE comparable to large commercial hybrid plants, highlighting manageability and energy complementarity benefits, potentially reducing storage-related (battery) costs over the project's lifespan.

Parrado et al. [47] analyzed the LCOE for different solar power setups in northern Chile's Atacama Desert: a $50\ MW$ standalone PV system, a $50\ MW$ standalone CSP system with $15$ hours of TES, and a PV-CSP hybrid system combining $20\ MW$ PV with $30\ MW$ CSP and $15$ hours of TES. Thanks to the area's abundant sunlight, the PV-CSP hybrid system is a reliable, eco-friendly solution for local industries such as mining. LCOE estimates showed significant reductions from $2014$ to $2050$, with the IEA Blue Map scenario dropping from $14.69$ to $8.57\ \$/kWh$ and the IEA Roadmap scenario from $13.88$ to $7.74\ \$/kWh$. While the hybrid system's LCOE is slightly higher than that of standalone systems, it provides continuous power and higher Capacity Factors, making it a promising option for stable, sustainable electricity and reduced carbon emissions in the region.

Furlan [48] explores the trade-offs between cost and environmental impact in hybrid systems combining CSP, TES, an auxiliary natural gas boiler, PV systems, and BESS. It highlights the uncertainties in energy resource prices and Global Warming Potential (GWP) indicators. Using robust multi-objective optimization, Monte Carlo simulations, and a fuzzy satisfying method, the study aims to minimize both Total Annualized Costs (TAC) and GWP. Results show an 82.7% reduction in GWP with only a 28% increase in TAC, demonstrating significant environmental benefits with modest economic impacts. Adjusting for natural gas price variability increases the optimal PTC area by 37% and reduces auxiliary boiler operation by 62%. The optimal design achieves a GWP of 36 kt$CO_2$-eq/year and reduces the LCOE by over 41% compared to standalone CSP systems in the Mojave Desert. However, the study's limitation is that it represents power-block operation only by overall efficiency without detailed simulation.

Ghirardi et al. [49] conducted a TRNSYS model to investigate the possible strategies to make solar energy more dispatchable and maximize its penetration in power grids with high contribution of renewables based on three solar technologies (PV, PTC and CRS) in the Arabian Peninsula. Thanks to the thermal storage system of concentrated solar energy, it has beneficial effect on the power dispatchability (75% the annual solar fraction for CSP only). In contrast, the dispatchability of electricity from PV is low; although it provides the cheapest solution. Hybrid solutions combine the benefits from both PV and CSP, keeping low the generation cost and ensuring a more flexible production.

### 1.3.6 Optimization

While some studies focus on the feasibility of renewable energy in a particular location [50], achieving a power balance [51] or sizing the system based on a mathematical model [52], most literature aims to find an optimal solution for the size of components of RES integrated ESS and energy management to maximize their benefits. Optimization surveys in the literature aim to minimize or maximize an economic or technical objective function. The objective function utilized in these studies includes cost of energy ($COE$), net present cost ($NPC$), fraction of energy supplied by the RES ($F_{RES}$), Loss of Power Supply Probability ($LPSP$), degradation, fuel consumption, and GHG emissions. Shayeghi et al. [53] have reviewed the objective function and classified it as either single or multi-objective functions.

Using an objective function to find the best solution has led researchers to implement various techniques. One of the most popular approaches is meta-heuristic techniques, including PSO, GA, ABC (Artificial Bee Colony), CSA (Cuckoo search algorithm), and others, due to their numerous benefits. These methods are independent of the initial solution and are derivative-free, making them more favorable, especially for multi-objective problems that are nonlinear and challenging to solve. For instance, Ngouleu et al. [6] proposed an optimal sizing approach for a standalone hybrid RES consisting of solar PV modules, wind turbines, battery and hydrogen-based saving using the four meta-heuristic methods. The objective function was to minimize the NPC. The results showed that out of all the battery and hydrogen-based storage systems, the PV/Wind/BESS stood out as the most financially feasible option.

In another study conducted by Adefarati et al. [54], the optimal cost utilization was determined in a system comprising PV modules, wind turbines, ESS, and a diesel generator, employing the fmincon algorithm. Through their research, the authors identified the minimum COE at $0.2716\ \$/\mathrm{kWh}$. Singh et al. [13] analyzed a grid-connected solar PV-fuel cell hybrid energy system to provide electricity to a small shopping complex in India with a total electricity demand of $135\ \mathrm{MWh/year}$. The optimal sizing of system components was determined using three meta-heuristic algorithms, and the results were compared in terms of cost-effectiveness. Based on the simulation outcomes, it was revealed that the combined power output of a $106\ \mathrm{kW}$ solar PV system, an $8\ \mathrm{kW}$ fuel cell, a $45\ \mathrm{kW}$ electrolyzer, and a $150\ \mathrm{kg}$ hydrogen tank would be sufficient to fulfill the total electricity demand. The results demonstrated that the suggested system is financially feasible, as the LCOE is calculated to be 0.104 $/kWh.

Moreover, Makhdoomi and Askarzadeh [12] focused on optimizing the design of an off-grid hybrid energy system with PV, diesel generator, and energy storage. The feasibility of different system configurations, including PV/diesel, PV/diesel/battery, and PV/diesel/Pumped Hydro Storage (PHS), was assessed using a multi-objective framework considering levelized cost of energy (LCOE) and Total Pollutant Emission (TPE) as problem objectives. Simulation results showed that the most cost-effective system was PV/diesel/PHS with fixed panels, with LCOE of 0.198 $/kWh. N'guessan et al. [34] determined the optimal size of a hybrid wind/fuel cell/battery/supercapacitor system using the NSGAII algorithm based on experimental data, and the optimization was done based on minimizing TAC and LPSP. The optimal solution was chosen based on finding a cost-effective set of system components that meet the desired reliability. The study showed that the lowest achieved TAC was approximately 11508 €/year, with a corresponding LPSP of 4.4 percent.

In addition, Samy et al. [15] investigated the use of combined renewable energy systems (CRES) in a small countryside area in Egypt using solar PV, wind, and fuel cell technologies. The study aimed to increase the share of renewable energy in the energy mix and explores the feasibility of using fuel cells as a storage/backup system instead of batteries. Three CRES combinations were compared using mathematical modeling and optimization techniques, and the most optimal system was identified. Furthermore, Akram et al. [55] proposed two constraint-based iterative search algorithms for optimal sizing of wind turbines, PV, and BESS in a grid-connected microgrid. The algorithms aimed to determine the optimal sizes of RES and BESS based on maximum reliability and minimum cost, while avoiding over- and under-sizing. Additionally, a modified CSA algorithm called CSAadaptive-AP was proposed to optimize hybrid energy systems, including PV, diesel generator, fuel cell, electrolyzer, and hydrogen tank, subject to reliability and renewable energy portion [56]. Maheri et al. [57] presented an integrated configuration-size optimization formulation that allows for finding the optimum configuration and size of components for a given site by solving one optimization problem. The formulation can also be used for retrofitting existing systems using the GA and NSGA-II to explore and exploit the design space. Akhavan et al. [58] also used GA method to minimize the annual total cost while balancing the high costs of renewable electricity generation.

Another research effort, conducted by Vaderobli et al [59], focused on optimizing PTC across different locations in the United States. Utilizing the innovative Better Optimization of Nonlinear Uncertain Systems (BONUS) algorithm, significant savings of $41\% - 47\%$ on LCOE were achieved, integrating weather and cost uncertainties into the optimization framework. Garge et al. [60] undertook a seven-dimensional optimization of a PTC-power block system, aiming for minimum investment cost per unit of nameplate electricity production. Parameters such as working fluid, heat source temperature, and condenser characteristics were considered, revealing that $R152a$ and isopentane were optimal under different conditions.

Esfahani et al [61], conducted an extensive assessment and optimization of a PTC system in Tehran, encompassing energy, exergy, exergoeconomic, and exergoenvironmental analyses. Results revealed that the PTC exhibited its highest energy efficiency $(73.6\%)$ in July and its highest exergy efficiency $(20.11\%)$ in January. Furthermore, a multi-objective GA was employed to optimize the PTC, enhancing design parameters and operating conditions. Optimization outcomes showcased that for January, which boasted the maximum exergy efficiency, the optimized PTC achieved an exergy efficiency of $26.38\%$ and a total cost of 0.61 $\$/h$. Lou et al. [62] develop a multilevel research methodology to explore the multidimensional performance of the solar thermal-PV hybrid microgrid to provide a stable and sufficient electric power supply for buildings. Configuration optimization is conducted across various dimensions, including regions, LCOE, and Loss of Load Probability (LOLP), and load types. The study suggests that hybrid microgrid configurations for buildings can improve solar energy utilization and decrease fossil fuel usage, providing an effective energy solution for distributed systems. However, in regions with limited solar energy, power load tracking may not be viable, but supplying the basic load remains a practical option.

Among the optimization methods, PSO is a metaheuristic technique that has gained popularity in solving complex optimization problems since this algorithm's implementation is easier, there is less need to adjust parameters, and the rate at which it converges is fast [63]. In particular, PSO has been applied to solve the Distributed Generation (DG) placement problem, which involves determining the best location and size of DG units in a distribution system to enhance power delivery and reliability [64]. According to Musa and Ibrahim [65], PSO has been found to be an efficient approach to handling DG placement and sizing problems. Their study reviewed the use of PSO algorithms and highlighted their effectiveness in solving the optimization problem.

Fodhil et al. [7] investigated the economic and performance results of a hybrid PV-diesel-battery system for load following dispatch strategy. The results showed that the PSO optimal system is more cost-effective and has more renewable penetration than the HOMER optimal system, while both systems are able to supply load consumption without any unmet load. In [10], the findings suggested that the most suitable sizing of BESS based on PSO provides superior dynamic stability compared to both the optimal sizing of BESS using an analytic method and the typical BESS sizing. Similarly, Mah et al. [11] proposed an optimization framework for designing and operating a standalone microgrid with electrical and hydrogen loads using a PSO algorithm. Based on their results, the optimal microgrid design had a high potential for energy waste due to oversized solar panels, and a cost reduction could be achieved by targeting only 95% of loads with LCOE ranges from 0.4551 \$/kWh to 0.4572 \$/kWh. García-Triviño et al. [66] compared three optimization algorithms (PSO, fmincon, and fminimax) to solve a multi-objective function with constraints related to net power. The results showed that PSO was the fastest and most effective algorithm for finding solutions.

The PSO method has been extensively utilized in various studies for optimization problems, including distributed generation placement and sizing problems [11, 16, 67]. However, despite its efficiency, PSO has certain limitations. One of its main challenges is the lack of a solid mathematical background, which is similar to many other heuristic methods. Additionally, the solution method of PSO is problem-dependent, and parameters need to be adjusted for each solution to achieve better optimization [65].

Moreover, the typical assumption that the inertia term is eliminated at an early stage of the optimization process can lead to the algorithm getting trapped in local minima [68]. To address these challenges, researchers have explored other versions of PSO or developed hybrid algorithms by combining multiple algorithms. The choice of using other versions of PSO or hybrid optimization depends on the specific problem being addressed. For instance, an optimized generation scheduling model was proposed for a wind-PV-EFCS hydrogen production system that integrated renewable power generation with hydrogen production and storage, as well as BESS [69]. The model is optimized using an adaptive simulated annealing PSO algorithm, which has a higher ability to find global optima compared to plain PSO. In another study conducted by Elnozahy et al. [14] a hybrid microgrid system utilized PV and wind energy, coupled with a hybrid BESS that included supercapacitors, hydrogen fuel cells, flywheels, and pumped hydro-storage. To optimize the system's performance, the researchers proposed a hybrid optimizer, namely PSO-GOA, to enhance the ordinary PSO exploration feature by incorporating the exploration of the GOA.

Moreover, Ziari et al. [70] combined PSO with GA to avoid trapping in a local optimum. Another limitation of plain PSO is that it can only handle unconstrained problems, and additional techniques need to be incorporated to handle constraints. Various techniques have been proposed, including the penalization method, which penalizes the function value associated with infeasible solutions to convert the original constrained problem into an unconstrained one. Other techniques, such as preserving feasibility and bisection methods, can also be specifically designed for

PSO. However, these techniques have their own drawbacks, such as being time-consuming for low feasibility ratios of the search space, lack of exploration of infeasible regions, possibility of converging to non-optimal but feasible solutions and limitations of passing through infeasible space [71]. While optimizing a simple objective function can yield satisfactory results, adopting a multicriteria formulation can offer a more realistic and reliable solution for practical situations, particularly in cases where continuous and reliable energy supply is of critical importance [72].

Despite significant progress in renewable energy systems (RES) and their integration with energy storage systems (ESS), several gaps persist in the current body of research.

- **Assumption of Power Block as a Single Unit**: Previous studies often assume the power block as a single unit, focusing on overall efficiency and rated power, without considering the individual component limitations and efficiencies.
- **Separate Optimization of PTC and Power Block**: There is a lack of integrated system consideration, as most studies optimize parabolic trough collectors (PTC) and power blocks separately.
- **Constant Output Power Assumption**: Many studies assume constant output power for the power block, failing to assess the system under varying conditions that reflect real-world scenarios.
- **Specific Design Day Optimization**: System optimizations are frequently based on a specific design day, ignoring the variability and fluctuations in actual operating conditions.
- **Neglect of Power Limitations**: Components such as electrolyzers, fuel cells, and hydro pumps often have their power limitations neglected in system assessments.
- **Single Efficiency Assumption for Integrated Units**: The assumption that electrolyzer, hydrogen tank, and fuel cell operate as a single unit with one efficiency overlooks the individual performance characteristics and constraints of each component.

In light of these gaps, this study aims to address several critical objectives and introduce innovative methods:

- **Minimizing Energy Costs**: The primary objective is to minimize energy costs while maintaining a specific renewable energy fraction.
- **Evaluating Hybrid Systems**: This study evaluates hybrid systems utilizing different and similar sources of renewable energies, specifically combinations of PV panels, wind turbines, and PTC systems.
- **Integration with Energy Storage Systems**: Assessing the integration of renewable energy systems with various energy storage systems, including batteries, electrolyzer-fuel cell systems (EFCS), and thermal storage tanks.
- **Techno-Economic Optimum Solution**: Achieving a techno-economic optimum solution by considering the capacities of PV, PTC, power block components (ORC), wind, battery, electrolyzer, hydrogen tank, and fuel cell as variables in the optimization process.
- **Realistic Operating Conditions**: Optimizing the power block under realistic operating conditions in the PTC/ORC system, accounting for the fluctuating efficiency of the ORC and the effect of partial load on turbine efficiency.
- **Introducing Constraints on Variables**: Incorporating constraints on variables, which are rarely considered in similar studies, making the optimization problem more nonlinear and challenging.
- **Hybrid PSO-GA Approach**: Proposing a hybrid Particle Swarm Optimization-Genetic Algorithm (PSO-GA) approach to effectively address the complexity of the optimization problem and present a robust and realistic method.

Overall, in this study, efforts were made to address the gaps identified in the literature by introducing a comprehensive and optimized method for designing effective renewable energy systems. Various hybrid systems were evaluated, and renewable energy sources were integrated with advanced energy storage solutions to provide a techno-economic optimum solution that is both feasible and efficient. The innovative hybrid PSO-GA optimization approach was employed to tackle the complexity of the design, ensuring realistic and robust outcomes. This research paves the way for the implementation of renewable energy systems in microgrids, contributing to sustainable and reliable energy solutions. Ultimately, this work aims to respond to the global challenges of energy demand and climate change, promoting the adoption of renewable energy and reducing the impact of global warming.

# CHAPTER 2

# METHODOLOGY

In this study, the PV system is examined in integration with two different ESS, including batteries and fuel cells. Additionally, it is assessed in hybrid systems that incorporate wind turbines and PTC systems to meet the electricity demand of the METU NCC campus. The PTC system is also evaluated independently. As a result, eight scenarios representing different integrated systems are investigated, as shown in Table 2.1. The objective is to determine the optimal capacity of components in each scenario based on the lowest weighted average cost of electricity (waCOE). For each combination of RES and ESS, techno-economic parameters are compared under grid-connected conditions.

The methodology employed in this study is comprehensively structured into ten subsections. Sections 2.1, 2.2 and 2.3 elaborate on the theoretical background of the PV system, wind turbine, and PTC, respectively. Section 2.4 discusses the ESS, including batteries and EFCSs. Section 2.5 covers the power block systems and the approach for partial load. Section 2.6 presents the economic and technical analysis conducted to assess the feasibility of the proposed systems. Section 2.7 explores the demand management approach in each scenario. Section 2.8 details the optimization methodology utilized, combining the PSO method with the GA method. Finally, Section 2.9 provides an overview of the case study conducted at METU NCC.

Table 2.1 Proposed scenario components

| Scenario | #1 | #2 | #3 | #4 | #5 | #6 | #7 | #8 |
|---|---|---|---|---|---|---|---|---|
| **RES** | **PV** | **PV** | **Wind** | **Wind** | **Wind + PV** | **Wind + PV** | **PTC** | **PV + PTC** |
| **ESS** | **BESS** | **EFCS** | **BESS** | **EFCS** | **BESS** | **EFCS** | **TES** | **BESS + TES** |

## 2.1 PV System Model

The energy generated by a PV system depends on the PV module's efficiency, $\eta_{PV}$, PV system efficiency, $\eta_I$, module number, $N_M$, module area, $A_M$, and incident total radiation on the tilted surface, $I_T$. This generated energy could be calculated by Eq. (2.1) [73].

$$E_{PV} = \eta_{PV} \times \eta_I \times A_M \times N_M \times I_T \tag{2.1}$$

where $\eta_I$ incorporates the system's losses, such as soiling, shading, and inverter losses that is obtained from the literature [74]; $A_M$ is considered based on the manufacturer's catalog, and module efficiency $\eta_{PV}$ is given by Eq. (2.2) as,

$$\eta_{PV} = \eta_{PV,ref} \times \left[1 - \left|\beta_{ref}\right| \times (T_{PV} - T_{STC})\right] \tag{2.2}$$

where $T_{PV}$ can be estimated by Eq. (2.3) as,

$$T_{PV} = T_{amb} + \frac{G_T}{G_{NOCT}} \times (NOCT - T_{aNOCT}) \tag{2.3}$$

Since $T_{PV}$ counts on the ambient temperature and solar insolation, the efficiency of the PV system is also affected by their values. The hourly value of the ambient temperature is available from the Typical Meteorological Year (TMY) weather data. To calculate the solar insolation on the tilted surface, the anisotropic HDKR method is implemented here using direct normal and diffuse horizontal irradiation values [75]. For brevity, their methodology is not duplicated here. The AXIPower-AC-250P/156-60S PV module is employed in this study as it is the module installed on the campus. Table 2.2 represents the technical information of the utilized PV module.

To maximize the annual energy output based on the TMY weather data, the tilt and azimuth angles are set to 30° and 0°, respectively.

Table 2.2 Technical specification of the AXIPower-AC-250P/156-60S PV module [76]

| Parameter | | Value | Unit |
|---|---|---|---|
| Nominal output | $P_{mpp}$ | 250 | $W_p$ |
| Module conversion efficiency | $\eta_{PV}$ | 15.37 | % |
| NOCT | $NOCT$ | 45 | °C |
| Temperature coefficient for power | $\beta_{ref}$ | 0.42 | %/°C |
| Single module area | $A_M$ | 1.63 | $m^2$ |
| PV system efficiency | $\eta_I$ | 86 | % |

## 2.2 Wind System Model

Wind power strongly depends on wind speed and duration [77]. The wind speed at hub elevation $u_Z$ is required which can be obtained by Eq. (2.4) utilizing shear coefficient, $\alpha$, which is assumed as $1/7$ [73]. In this equation, $u_g$ reperesents wind speed at reference level, $Z$ and $Z_g$ denote the height of the wind turbine hub and height of the reference level, respectively.

$$u_Z = u_g \times \left(\frac{Z}{Z_g}\right)^{\alpha} \tag{2.4}$$

By this, the output electrical power of a wind turbine can be calculated by Eq. (2.5),

$$P_e = \begin{cases} 0 & for \;\; u_Z < u_{cut-in} \; or \; u_Z > u_{cut-out} \\ P_{rated} \times \dfrac{(u_{cut-in})^k - (u_Z)^k}{(u_{cut-in})^k - (u_{rated})^k} & for \;\; u_{cut-in} \le u_Z \le u_{rated} \\ P_{rated} & for \;\; u_{rated} < u_Z \le u_{cut-out} \end{cases} \tag{2.5}$$

where $k$ is given by Eq (2.6) [78]:

$$k = \left(\frac{\sigma}{\bar{u}}\right)^{-1.086} \qquad for\ 1 \leq k \leq 10 \tag{2.6}$$

The utilized wind turbine model in this study is VESTAS V90-2.0 MW IEC IIA/IEC S, whose technical information is obtained from the manufacturer's catalog as provided in Table 2.3

Table 2.3 Technical specifications of the VESTAS V90-2.0 MW IEC IIA/IEC S wind turbine [79]

| **Parameter** | | **Value** | **Unit** |
|---|---|---|---|
| **Rated power** | $P_{rated}$ | 2 | MW |
| **Cut-in speed** | $u_{cut-in}$ | 4 | $\mathrm{m/s}$ |
| **Cut-out speed** | $u_{cut-out}$ | 25 | $\mathrm{m/s}$ |
| **Rated speed** | $u_{rated}$ | 15 | $\mathrm{m/s}$ |
| **Hub height** | $Z$ | 80 | m |

## 2.3 PTC System Model

The useful energy output of the PTC system, $\dot{Q}_{u,PTC}$, relies on several factors, including the collector's efficiency $\eta_{PTC}$, aperture area $A_a$, number of loops $N_L$, number of collectors, $N_C$, and incident direct normal solar radiation, $I_{DNI}$. This energy is quantified by Eq. (2.7) [73].

$$\dot{Q}_{u,PTC} = \eta_{PTC} \times A_a \times N_L \times N_C \times I_{DNI} \tag{2.7}$$

The efficiency of the collector is determined using Eq. (2.8), derived from experimental data [80].

$$\eta_{PTC} = 0.7408 - 4.7851 \times 10^{-5} \Delta T_f - 5.58399 \times 10^{-7} \Delta T_f^2 \tag{2.8}$$

The efficiency calculation incorporates the temperature difference between the average Heat Transfer Fluid (HTF) temperature, $T_{HTF,avg}$ and the ambient temperature, $T_{amb}$, as denoted by $\Delta T_f$ in Eq. (2.9).

$$\Delta T_f = T_{HTF,avg} - T_{amb} = \frac{T_{Hst} + T_{Cst}}{2} - T_{amb} \tag{2.9}$$

Parameters such as the cold storage temperature ($T_{Cst}$) and hot storage temperature ($T_{Hst}$) are constants obtained through power block optimization, detailed in Section 2.5.

The flow rate heated by the PTC system is calculated using equation Eq. (2.10),

$$\dot{m}_{PTC} = \frac{\dot{Q}_{u,PTC}}{C_{p,ave} \times (T_{Hst} - T_{Cst})} \tag{2.10}$$

Additionally, the hourly quantities of HTF stored in the hot and cold storage tanks are determined by equations Eq. (2.11) and Eq. (2.12), respectively.

$$M_{Hst}(t+1) = M_{Hst}(t) + \dot{m}_{PTC}(t) \times 3600 \tag{2.11}$$

$$M_{Cst}(t+1) = M_{Cst}(t) - \dot{m}_{PTC}(t) \times 3600 \tag{2.12}$$

Table 2.4 represents the technical information of the utilized PTC module, HTF and TES.

Table 2.4 List of the parameters used for the design of the PTC, storage tank and power block

| Parameter | Unit | Value | Ref. |
|---|---|---|---|
| Collector Type | - | $Luz\ LS-3$ | [81] |
| Collector aperture width | $m$ | 5.75 | [81] |
| Collector module length | $m$ | 8.33 | [81] |
| Inner diameter of absorber tube | $m$ | 0.066 | [81] |
| PTC heat transfer and storage material | - | $Molten\ Salt$ $(60\%\ NaNO_3\ +\ 40\%\ KNO_3)$ | [81] |
| Density of molten salt | $\frac{kg}{m^3}$ | $2089.905 - 0.636\,T$ (°C) | [82] |
| Specific heat of molten salt | $\frac{J}{kg.K}$ | $1443 + 0.172\,T$ (°C) | [82] |
| Kinematic viscosity of molten salt | $\frac{m^2}{s}$ | $-6.557 \times 10^{-14}\,T^3 + 1.05 \times 10^{-10}\,T^2 - 5.706 \times 10^{-8}\,T + 1.112 \times 10^{-5}$ (°C) | [82] |
| Heat storage's depth of discharge | % | 90 | |

## 2.4 Energy Storage Components

The proposed RESs are coupled with two different storage systems, BESS and EFCS. In the integrated storage system, such as batteries, charge/discharge power is dependent on energy storage capacity [83]. The depth of discharge of the battery (DOD) represents the maximum fraction of the energy which could be extracted from the battery to avoid the inverse effects on its lifespan. Table 2.5 includes the technical specification of the utilized battery.

EFCS consists of three separated components, electrolyzer, hydrogen storage tank, and fuel cell. Electrolyzer is a device that converts electricity into chemical energy. Indeed, through the electrolysis process, water is converted to hydrogen and oxygen. The produced hydrogen is stored in the tank and whenever it is necessary to meet the deficit energy by ESS, the fuel cell starts to convert the chemical energy stored in the form of hydrogen into electricity. The output of the chemical reaction in the fuel cell is water vapor. The technical properties of the EFCS are represented in Table 2.5.

Table 2.5 Technical specifications of BESS [84] and EFCS [85]

| **BESS** | | **EFCS** | |
|---|---|---|---|
| DOD | 95 % | Electrolyzer efficiency | 95 % |
| Charge-discharge efficiency | 92 % | Fuel cell efficiency | 92 % |

## 2.5 Power Block System Model

The power block system, depicted in Figure 2.1, consists of ORC units and their associated thermodynamic states. The $T - S$ diagram of the ORC system is presented in Figure 2.2. Within the ORC, the working fluid undergoes compression from a saturated liquid to a high-pressure subcooled liquid (process 1–2) via a feed pump. In a recuperative ORC configuration, the subcooled liquid at state point 2 absorbs heat (process 2–9) from the exhausted vapor (process 6–8) within the recuperator.

Subsequently, the liquid at state point 9 enters the evaporator to absorb heat from the HTF. The position of state point 9 varies depending on operational parameters. The liquid then undergoes preheating, evaporation, and superheating (process 9–3, 3–4, and 4–5, respectively) before expansion in the turbine (process 5–6) to generate power. The exhausted gas re-enters the recuperator to transfer heat (process 6–8) to the working fluid, which then undergoes cooling and condensation (process 8–7 and 7–1) in a condenser, completing the cycle.

The ORC efficiency is determined by Eq. (2.13), requiring the calculation of heat energy received by the working fluid in the evaporator, $\dot{Q}_{evap}$, turbine output power, $P_T$, and cycle and condenser pump input power, $P_P + P_{P,cond.}$. Thus, knowledge of the enthalpy of each thermodynamic state point is essential. Table 2.6 outlines the state point of the working fluid in the components, process types, and known variables aiding in enthalpy determination.

$$\eta_{ORC} = \frac{P_T - P_P - P_{P,cond.}}{\dot{Q}_{evap}} = \frac{P_{net,ORC}}{\dot{Q}_{evap}} \tag{2.13}$$

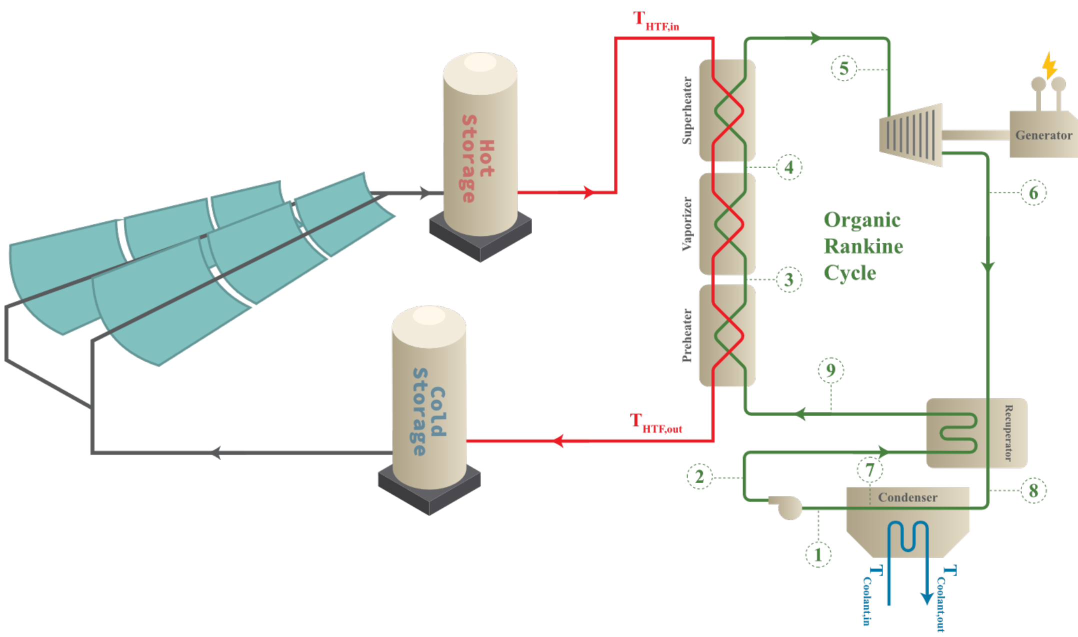


Figure 2.1. PTC-ORC system with two tanks direct thermal energy storage system

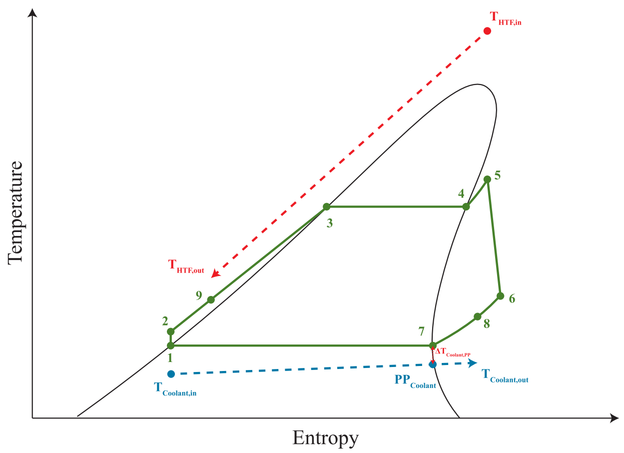


Figure 2.2. Thermodynamic cycle of ORC

Table 2.6 State point of the working fluid in the components, process types, and known variables

| State Point | Component | Known Properties |
|---|---|---|
| 5 | Turbine Entrance | $P_5, T_5$: Determined by optimization |
| 6 | Turbine Exit | $P_6 = P_7$<br>$h_6 = h_5 - \eta_{T,is} \times \left(h_5 - h_{6,is}\right)$ |
| 7 | Condenser Pinch Point | $x_7 = 1$<br>$T_7 = T_{coolant,in} + \Delta T_{coolant} + \Delta T_{Coolant,PP}$ |
| 1 | Condenser Exit and Pump inlet | $x_1 = 0$<br>$T_1 = T_7$ |
| 2 | Pump Exit | $P_2 = P_5$<br>$h_2 = \frac{\left(h_{2,is} - h_1\right)}{\eta_{P,is}} - h_1$ |
| 3 | Preheater Exit and Vaporizer Inlet | $x_3 = 0$<br>$P_3 = P_5$ |
| 4 | Vaporizer Exit and superheater Inlet | $x_4 = 1$<br>$P_4 = P_5$ |

Starting from state point 5, temperature and pressure determined by the optimizing, below the critical state point (Section 1.6), facilitate enthalpy calculation. At state point 6, the turbine's isentropic efficiency aids in obtaining the actual enthalpy, with pressure assumed equal to state point 7 due to constant pressure in heat exchangers.

State point 7's thermodynamic state is determined based on vapor quality and temperature. In the context of heat exchangers, the pinch point refers to the location where the temperature difference between the working fluid and the cooling/heating fluid is minimized. In the condenser, although the temperatures at state points 1 and 7 are equal, the cooling water temperature rises from the entrance to state point 7, indicating that state point 7 is the pinch point where the temperature difference between the working fluid and the cooling fluid is minimized, Figure 2.2. By knowing the temperature of the cooling water at the inlet, the temperature increment of the cooling water up to the pinch point, and the value of the pinch point as the input, the temperature of state point 7 can be calculated, Table 2.6.

State point 1 mirrors state point 7's temperature and represents the condenser's outlet with zero vapor quality. State point 2, the pump exit, shares pressure with state point 5. The pump's isentropic efficiency aids in determining state point 2's actual enthalpy.

Knowing the pressure in state points 3 and 4, identical to state point 5, and their vapor qualities of 0 and 1, respectively, assists in determining their enthalpies.

The remaining state points, 8 and 9, located at the exit of the working fluid in the upper and lower sides of the recuperator, require investigation. The location of state point 9 may vary between processes 2–3, 3–4, or even 4–5, contingent upon operational parameters.

a) If state point 9 located between state points 2 and 3

In the recuperator, the saturated vapor exiting the turbine enters at state point 6 and exits at state point 8 after transferring energy to the working fluid passing through state points 2 to 9, Figure 2.3a. The pinch point lies between 6 and 9 or 8 and 2, allowing for calculation of the thermodynamic properties of state points 8 and 9.

Considering the evaporator, with state point 9 between state points 2 and 3, the working fluid enters at state point 9 and exits at state point 5 after receiving energy from the HTF. As the enthalpy of state point 9 is lower than that of state point 3, the pinch point lies between state points 9 and $T_{HTF,out}$ (which is equal $T_{Cst}$) or state point 3 and $T_{Eva,PP}$, Figure 2.3a. Thus, the mass flow rate of HTF and $T_{HTF,out}$ calculated as depicted in Figure 2.4.

b) If state point 9's temperature is equal or greater than that of state point 3

In this case, the pinch point in the recuperator lies between state points 8 and 2 or state point 3 and $T_{Recup,PP}$, Figure 2.3b, allowing for the determination of the properties of state points 8 and 9.

For the evaporator, the pinch point is between state point 9 and $T_{HTF,out}$, enabling calculation of the mass flow rate of HTF, Figure 2.4.

c) If state point 9's temperature is less than that of state point 2

In this case, the recuperator is absent, and the subcooled working fluid directly enters the evaporator.

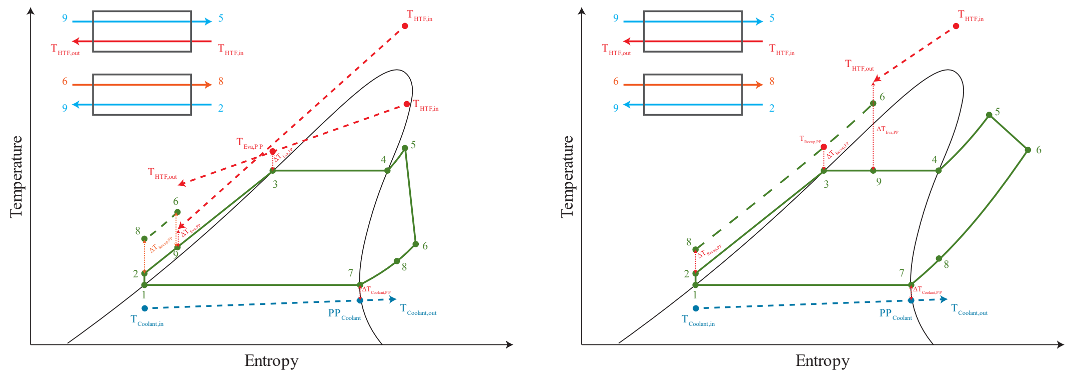


(a) (b)

Figure 2.3. Different possible position of state point 9 depending on operational parameters and identical pinch points in recuperator and evaporator

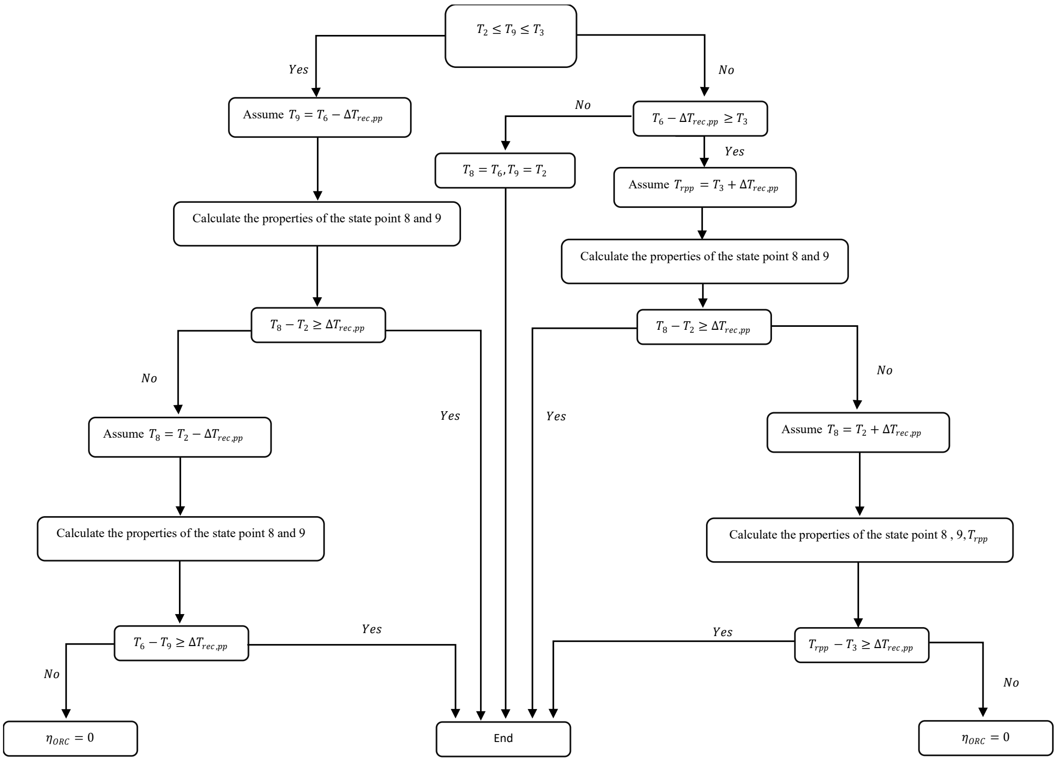


Figure 2.4. Optimization flowchart of ORC [86]

### 2.5.1 Partial Load

In this investigation, the maximum power output of the ORC system is constrained to its rated power. Consequently, there are periods during operation when the turbine operates below its full capacity, referred to as partial power, dictated by varying mass flow rates of the working fluid. The turbine's power output for any mass flow rate of the working fluid is determinable through the Willans' line equation [87], serving as a reliable predictor for turbine performance at partial loads, Eq. (2.14).

$$P_T = a + b \times \dot{m}_{ORC} \tag{2.14}$$

Suppose the constant term (referred to as $a$ in Eq. (2.15)) of the Willans' line equals y times the rated power output of the turbine:

$$a = -y \times P_{T,D} \tag{2.15}$$

The value of $b$ can be derived from the following relationship:

$$b = (1 + y)\frac{P_{T,D}}{\dot{m}_{ORC,D}} \tag{2.16}$$

## 2.6 Economic and Technical Analysis

The weighted-average cost of electricity (waCOE) is a crucial metric for assessing the economic viability of energy systems in this study. Unlike conventional methods like Levelized Cost of Electricity (LCOE), which considers total generated energy, waCOE incorporates the unit cost of self-consumed produced electricity (CosE). CosE specifically accounts for demand energy covered by renewable sources, reflecting the one-way tariff system in place, where excess energy is injected into the grid without revenue for the producer. Equation (2.17) outlines the calculation of CosE:

$$CosE = \frac{C_i + \sum_{t=1}^{l}\frac{M_t}{(1+r)^t}}{\sum_{t=1}^{l}\frac{P_{RES}}{(1+r)^t}} \tag{2.17}$$

The system components, except the battery, are assumed to have a uniform lifetime of 30 years. The battery's lifetime is set to 10 years, and the cost of battery replacement is factored into CosE calculations. Investment costs encompass both component and installation expenses. Economic parameters utilized in this study are detailed in Table 2.7.

In the proposed system, any energy shortfall not met by renewable sources is procured from the grid at a tariff of 0.210 €/kWh. The metering system operates unidirectionally, allowing surplus generation beyond what can be stored in ESS to be injected into the grid free of charge. Considering these conditions, the final waCOE is determined by:

$$waCOE = \frac{P_{RES}\times CosE + P_{Grid}\times GT}{D} \tag{2.18}$$

where $P_{RES}$ is demand energy covered by renewable sources.

This approach ensures a more accurate, realistic, and logical assessment of economic feasibility compared to traditional methods.

The RES Fraction ($F_{RES}$) and Demand-Supply Fraction ($DSF$) are the technical benchmarks that enable decision-makers to investigate and compare different systems with each other and are employed here as well. $F_{RES}$ represents how much of the demand energy could be supplied by the RES with or without ESS, and $DSF$ is a parameter that reveals the autonomy of the system based on time. These two parameters obtain from Eq. (2.19) and Eq. (2.20), respectively [9].

$$F_{RES} = \frac{P_{RES}}{D} \tag{2.19}$$

$$DSF = \frac{H}{24 \times 365} \tag{2.20}$$

where $H$ is yearly number of hours which the energy system covered the demand. In this study, the time step is considered as an hour.

Table 2.7 Economic parameters of the PV, battery, PTC and ORC system

| Component | Unit | Value |
|---|---|---|
| Modules and HTF cost | $\$/m^2$ | 280 |
| Heat storage material cost | $\$/kg$ | 0.49 |
| Heat storage cost | $\$/kWh$ | 31.1 |
| Land and site development cost | $\$/m^2$ | 6 |
| Civil works cost | $ | $169(kW_e) - 0.00053(kW_e)^{0.75}$ |
| Miscellaneous cost | $\$/kW_e$ | 183 |
| Turbine cost | $ | $1{,}467{,}000\left(\frac{n}{n_0}\right)^{0.5}\left(\frac{SP}{SP_0}\right)^{1.1}$ $SP_0 = 0.18\,m, n_0 = 2$ |
| Generator cost | $ | $2447(kW_e)^{0.49}$ |
| Condenser cost | $ | $597(kW_{th})^{0.68}$ |
| Pump cost | $ | $16{,}800(kW_e/200)^{0.67}$ |
| Heat exchanger cost | $ | $235(kW_{th})^{0.75}$ |
| Annual solar field component replacement cost | $\$/year$ | 2.5% of solar field cost |
| Annual operation and O&M cost | $\$/year$ | 4% of equipment cost |
| PV system capital cost | €/kW | 1547 |
| Annual PV O&M cost | €/kW | 24 |
| Wind system capital cost | €/kW | 1175 |
| Annual wind O&M cost | €/kW | 35.25 |
| Electrolyzer capital cost | €/kW | 4600 |
| Annual electrolyzer O&M cost | €/kW | 138 |
| Hydrogen fuel cell capital cost | €/kW | 3947 |
| Annual fuel cell O&M cost | €/kW | 118.41 |
| Hydrogen tank capital cost | €/kg | 470 |
| Annual hydrogen tank O&M cost | €/kg | 9.4 |
| Battery capital cost | €/kWh | 550 |
| Annual battery O&M cost | €/kWh | 10 |
| Life time | $year$ | 30 |
| Discount rate | % | 9 |

## 2.7 Demand Management Approaches

In this section, the demand management strategies for each system are discussed. The strategies include the prioritization and limitations of using RES and ESS. It also outlines when energy should be imported from the grid and when the RES should export energy to the grid at no cost. This section is divided into two main parts:

1. Demand Management in PV+ESS, Wind+ESS, and Hybrid PV+Wind+ESS Systems: This part focuses on the demand management strategies for systems combining PV with ESS, wind turbines with ESS, and hybrid PV and wind systems with ESS, as they share similar strategies.
2. Demand Management in PTC and Hybrid PV+PTC Systems: This part describes the demand management strategies for systems using only PTC and hybrid PV+PTC systems, which have a distinct but consistent demand management approach.

### 2.7.1 Demand Management in PV+ESS, Wind+ESS, and Hybrid PV+Wind+ESS Systems

Figure 2.5 and Figure 2.6 shown the schematic of RES system integrated with BESS and EFCS, respectively. The corresponding energy management strategy flowchart for these systems are represented in Figure 2.7 and Figure 2.8. Overall, in both systems, the model determines if the amount of energy generated by the RES within the time step is sufficient to meet the demand. When the demand exceeds the step duration production, the energy storage fills the energy deficit. If there is not enough stored energy, the remaining needed energy is supplied by the grid. Besides, if the energy generated by the RES exceeds the demand, the model checks the capability of the storage system for storing the excess energy considering the battery/electrolyzer-tank capacity in each storage system.

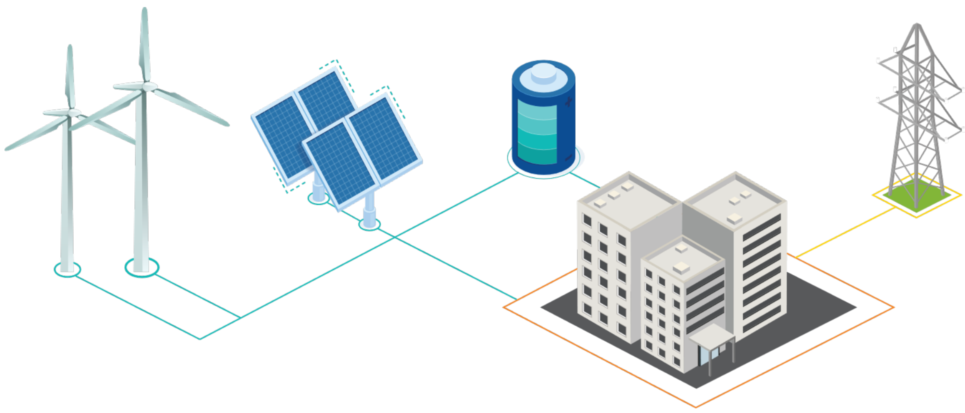

Figure 2.5. Schematic of energy system integrated with BESS

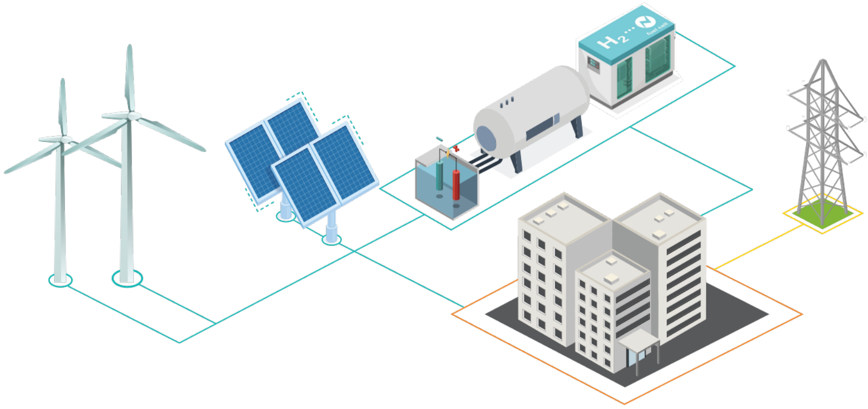

Figure 2.6. Schematic of energy system integrated with EFCS

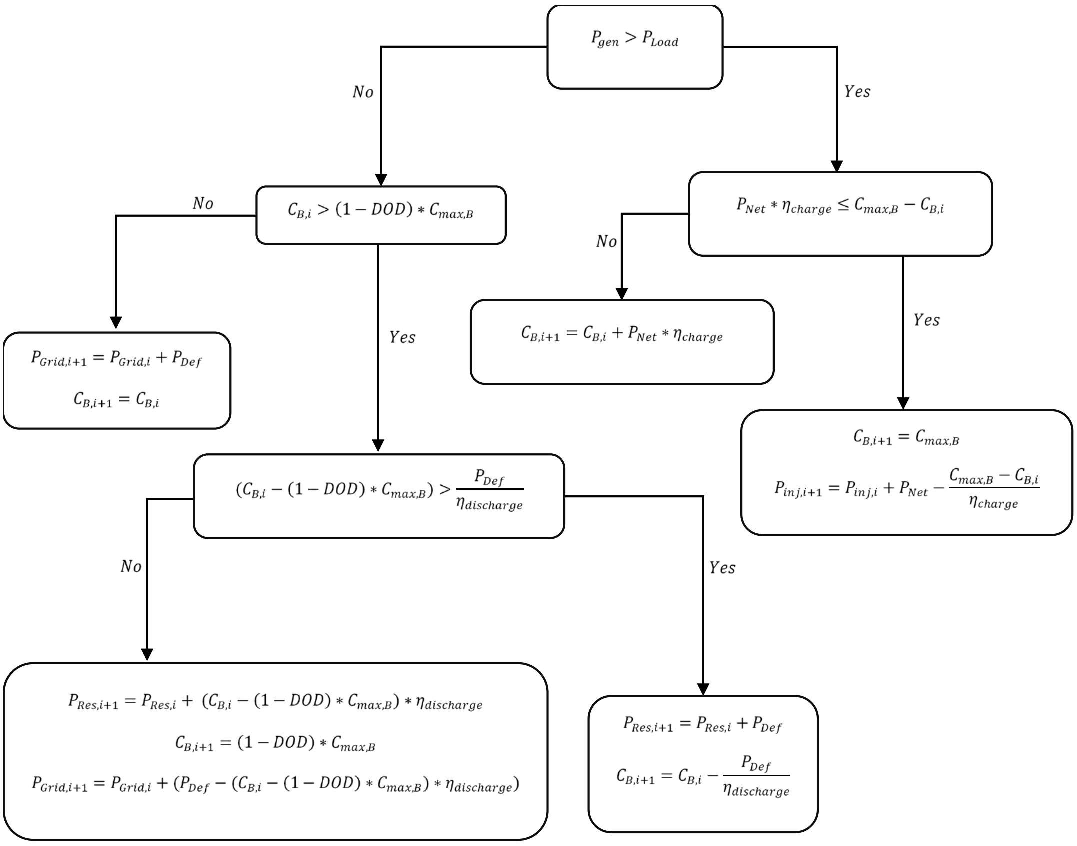


Figure 2.7. The energy system flowchart with BESS

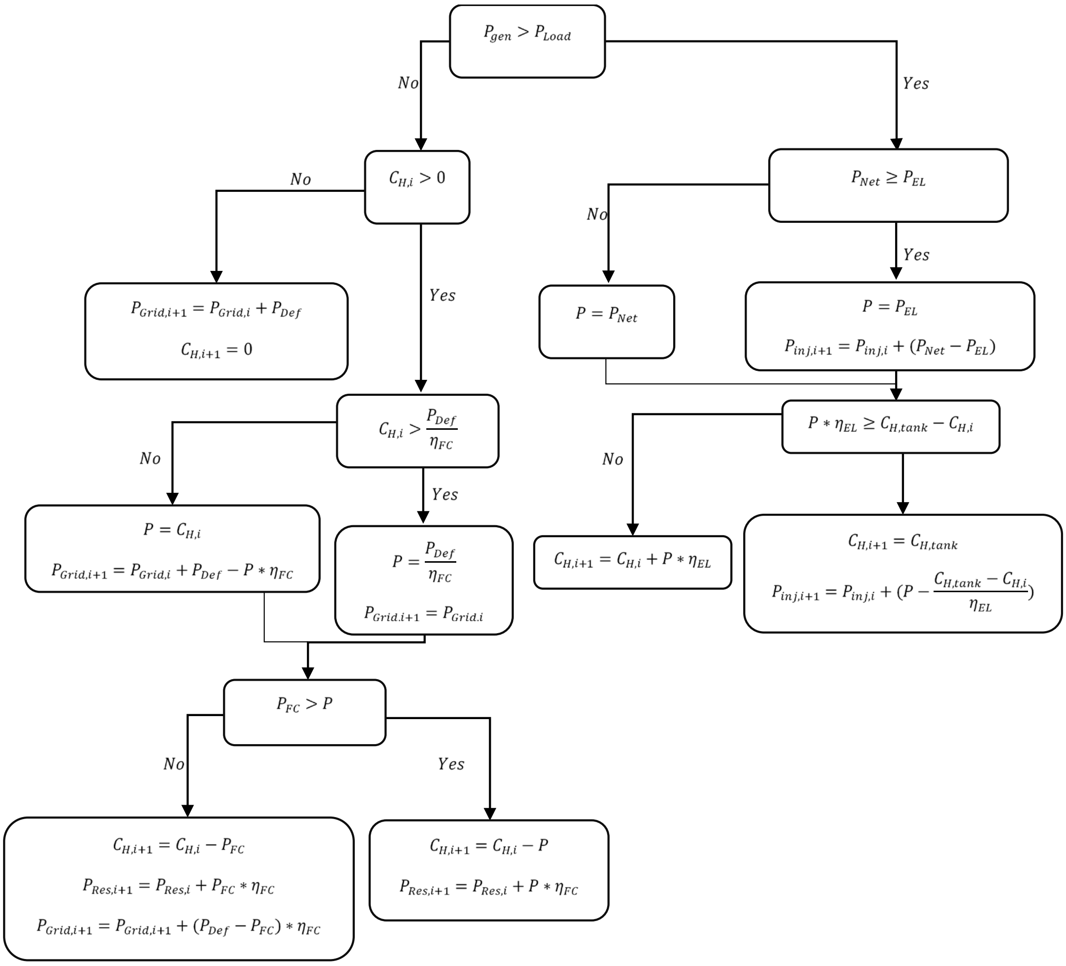


Figure 2.8. The energy system flowchart with EFCS

### 2.7.2 Demand Management in PTC and Hybrid PV+PTC Systems

In the PTC system, solar energy heats a heat transfer fluid (HTF) within the PTC, which is then stored in a hot tank. When demand arises, the stored hot fluid transfers its thermal energy to the power block's working fluid through the heat exchanger. The cooled thermal fluid is then stored in a cold tank. If the stored hot fluid or ORC generated power proves inadequate, the energy deficit is supplemented from the grid. Additionally, if the cold tank reserves are insufficient due to HTF total mass limitation, the PTC system ceases operation. HTF ensuring constant temperature in the storage tanks, facilitates heat transfer. Notably, the mass flow rate of the HTF may differ from hour to hour due to varying solar irradiation. The energy system flowchart of the only PTC system is showed in Figure 2.9.

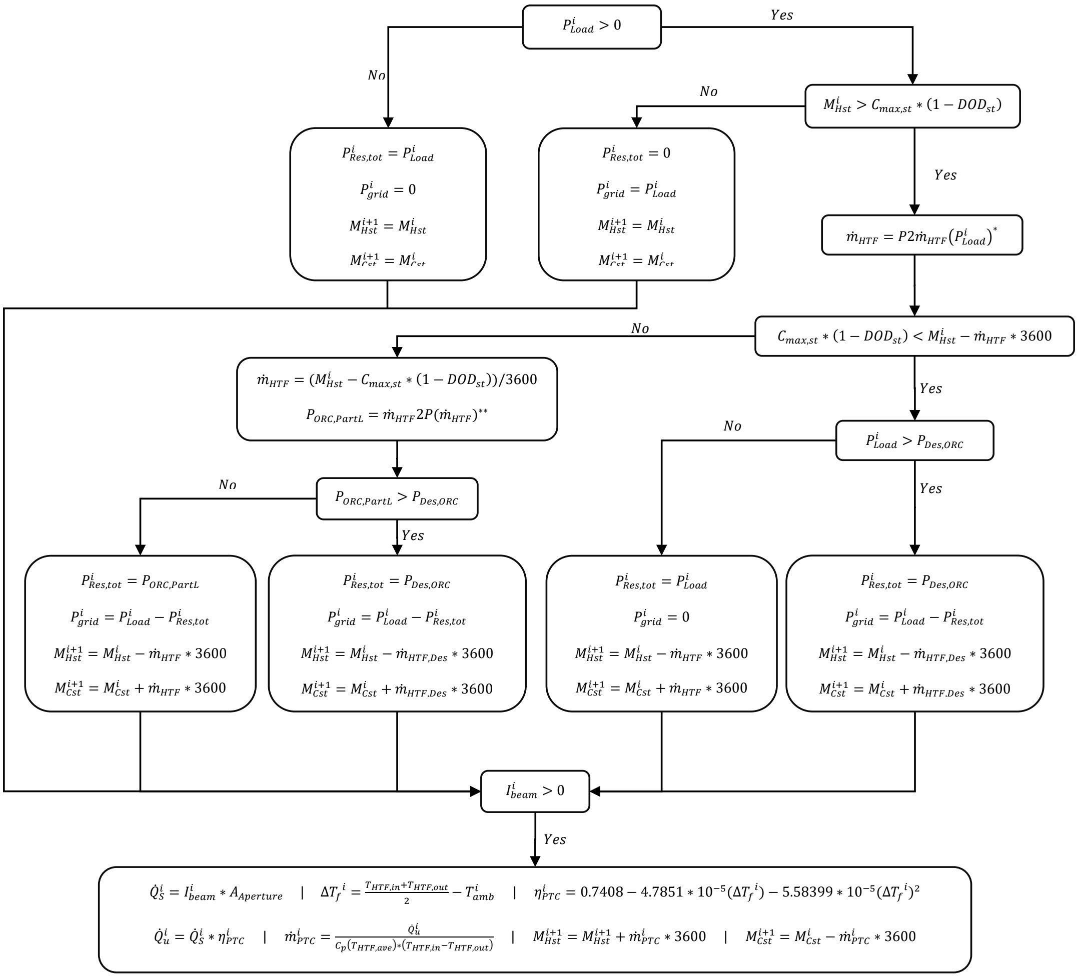


*The formula denotes the mass flow rate required to generate the power output of $P_{Load}^{i}$.

**The formula denotes the power produced by the mass flow rate of $\dot{m}_{HTF}$.

Figure 2.9. The energy system flowchart with PTC-ORC

The hybrid PV-BESS-PTC system combines elements of both technologies, Figure 2.10. Daytime demand is primarily met by the PV system, with excess electricity stored in batteries. The PTC system operates during daylight hours, storing thermal energy in the hot tank for using during the nighttime or periods of low solar radiation. Energy deficits during the shortage hours, met by battery reserves, ORC, and grid supply, respectively, depending on factors such as deficit magnitude and ESS state of charge. Figure 2.11 represents the energy system flowchart of the hybrid PV-BESS-PTC.

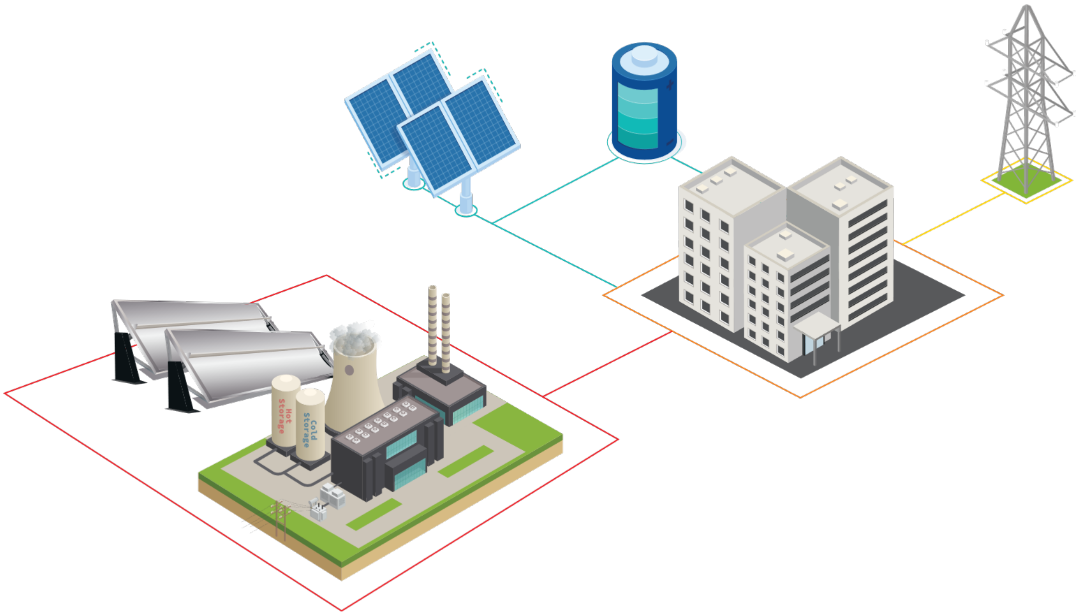


Figure 2.10. Hybrid PV- PTC -Battery RES

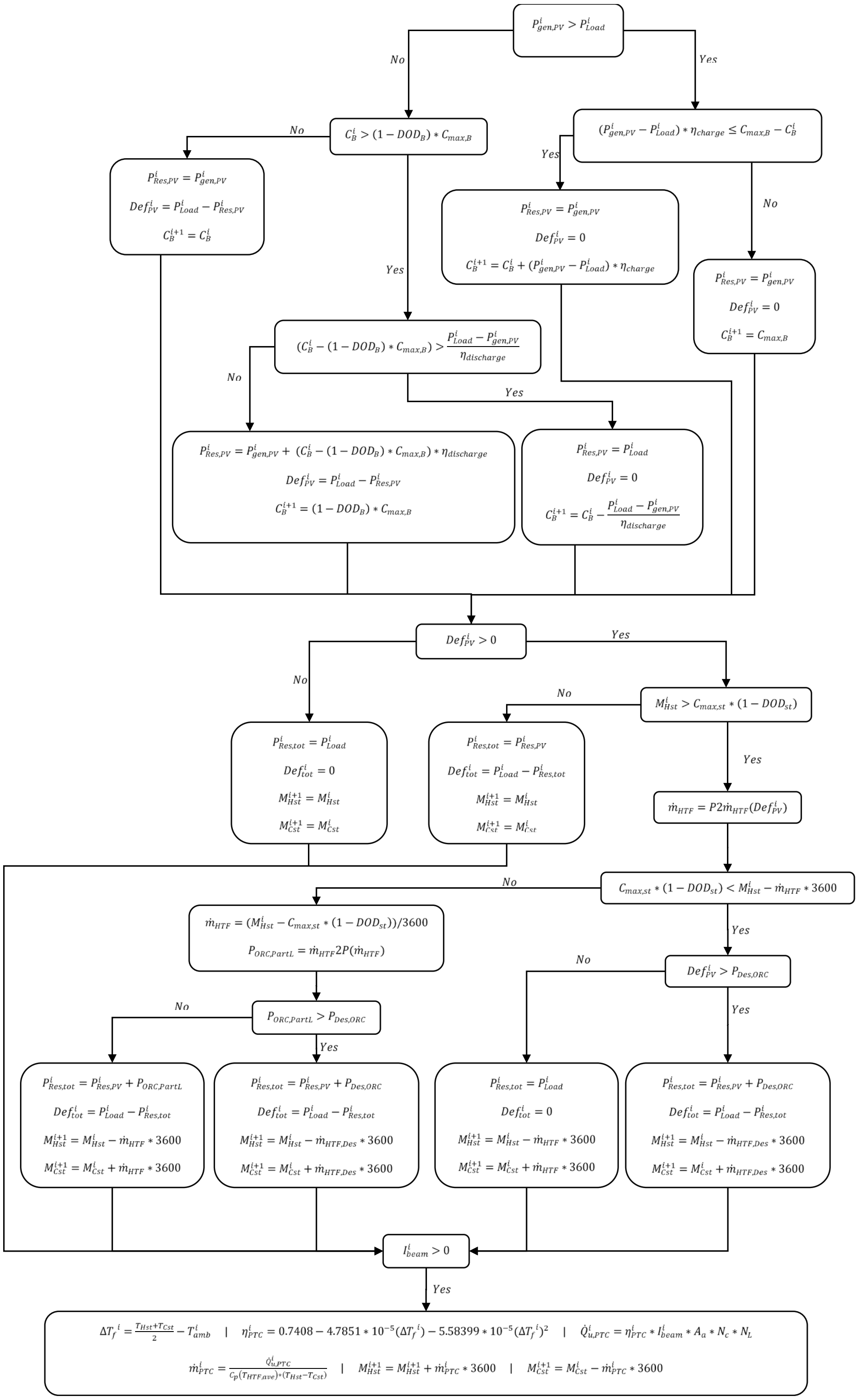


Figure 2.11. The energy system flowchart with PV-BESS-PTC system

#### 2.7.2.1 Technical Assumptions

In the analysis of system performance, several operational assumptions were made:

1. The system was analyzed under steady-state conditions to ensure consistency [88].
2. ORC works below the critical state points.
3. Negligible pressure drop and heat dissipation were assumed for tubes and heat exchangers [89].
4. Heat loss from thermal storage tanks was disregarded [90].
5. ORC maximum output power limited to rated output power
6. Turbine efficiency and thus generated power decrease under the partial load condition

Additionally, specific operational parameters were set:

1. The thermophysical properties of the working fluid are detailed in Table 3.
2. A pinch point temperature difference of 20 °C was established for heat exchangers (i.e., evaporator, recuperator, and condenser) [86].
3. The cooling water temperature at the condenser inlet was assumed to be 15 °C, rising by 10 °C at the pinch point, resulting in a selected condensation temperature of 45 °C for the ORC.

These operational assumptions and parameters are summarized in Table 2.8.

Moreover, it was ensured that the pressure and temperature upper limits of the superheated vapor at the turbine inlet were below the critical state point of the working fluid. Additionally, the lower temperature limit was set to ensure dry expansion of the vapor in the turbine. These measures guarantee safe and efficient operation of the system.

Table 2.8 Operational assumptions of the system

| Parameter | Unit | Value |
|---|---|---|
| Pinch point temperature difference in condenser | ℃ | 20 |
| Pinch point temperature difference in recuperator | ℃ | 20 |
| Cooling water inlet temperature | ℃ | 15 |
| Cooling water temperature at pinch point | ℃ | 25 |
| Turbine efficiency | % | 80 |
| Feed pump efficiency | % | 75 |
| Generator efficiency | % | 97 |
| Pump motor efficiency | % | 75 |
| Condenser pump pressure head | $m$ | 10 |

## 2.8 Optimization Method

The aim of this study is to optimize the capacity of RES components, such as PV modules, wind turbine, number of PTC modules and loops, heat storage capacity, and power block components such as turbine size, pump, evaporator, condenser, and recuperator, battery capacity, electrolyzer, hydrogen tank and fuel cell, based on the lowest $waCOE$. Each scenario considers a different combination of components, each with their own technical and economic characteristics. The varying solar and wind potential, as well as their intermittency, considering the fluctuating efficiency of the ORC and the impact of partial load on turbine efficiency add complexity to the problem, making it multidimensional and nonlinear. To tackle this challenge, a combination of simulation modeling and optimization methods is employed. MATLAB and EES is used to model the system components and simulate each scenario, and the PSO method is coupled with the GA method to find the optimal capacity of all components in each scenario.

In this section, the PSO method is introduced first, followed by the GA model. Subsequently, the proposed novel hybrid PSO-GA approach is discussed, and the implementation of this approach for solving the problem is explained.

### 2.8.1 Particle Swarm Optimization

PSO method considers the particles that each of them has a position (one of the possible solutions of the optimization problem) in the domain of the problem and move in this space. The motion law of these particles is fixed for all, and they all use their own previous experiences and other particles' previous experiences in their movement until the specified criteria reach their minimum or maximum value [91].

Each particle has five properties:

$X_i(t)$: Position

$Cost_i(t)$: The value of the objective function corresponding to the position

$V_i(t)$: Velocity

$X_{i,best}(t)$: The best position experienced by the particle so far

$Cost_{i,best}(t)$: The value of the objective function corresponds to the best position experienced by the particle so far

Velocity indicates the direction of motion since it is tangent to it. In fact, velocity is the direction that moves a particle from the previous position into the current position. In PSO, particles are self-organized. Indeed, in each iteration, the particle must move in three directions until reaching a new position:

1) Some in the direction of its current motion

2) A little towards its best memory

3) Some towards the best memory of all particles

Figure 2.12 illustrates these directions in a visual form.

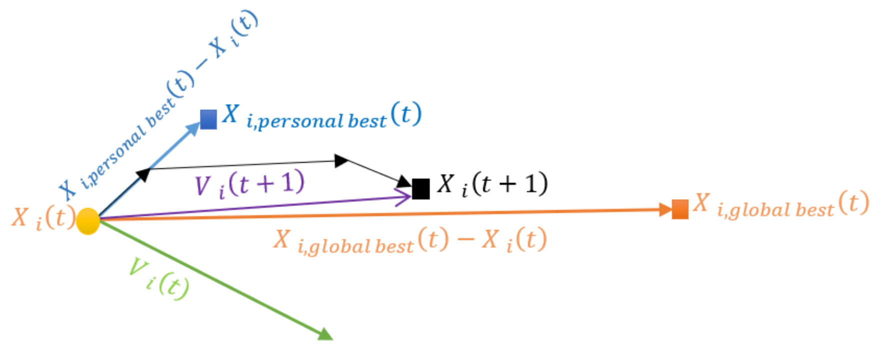


Figure 2.12. Three directions which a particle moves until reaching a new position: Some in the direction of its current motion, A little towards its best memory, Some towards the best memory of all particles

Then, the velocity and position of a particle are obtained by Eq. (2.21) and Eq. (2.22), respectively:

$$V_i(t+1) = wV_i(t) + c_1 r_1 \left(X_{i,personal\ best}(t) - X_i(t)\right) + c_2 r_2 \left(X_{i,global\ best}(t) - X_i(t)\right) \tag{2.21}$$

$$X_i(t+1) = X_i(t) + V_i(t+1) \tag{2.22}$$

In Eq. (2.21), $w$ is called the inertia coefficient. It is a coefficient that relates the current direction to the next direction. In other words, it indicates the tendency of the particle to maintain its current state of motion. This number should be less than 1 and the appropriate value of it is a number between 0.4 and 0.9. The lower inertia is, the faster the algorithm converges; and the higher it is, the higher the sudden motions happen. $r_1$ and $r_2$ are two random numerical vectors between 0 and 1 with a uniform distribution. $c_1$ and $c_2$ are called learning coefficients. $c_1$ is the coefficient of individual learning and $c_2$ is the coefficient of global learning. It is common for $c_1$ and $c_2$ to be non-negative numbers with a maximum of 2. Thus:

$$w \in [0.4, 0.9] \tag{2.23}$$

$c_1 \in [0,2]$ (2.24)

$c_2 \in [0,2]$ (2.25)

In optimization algorithms, there are two important concepts: exploration, which means the ability to generate new answers and random search, and exploitation, which means the ability to cultivate current answers and local search. Accordingly, increasing $w$ and $c_1$ are in favor of exploration while increasing $c_2$ improves the exploitation of optimization method. Therefore, optimization algorithms are usually implemented in such a way that at the beginning, the exploration rate is high and the exploitation rate is low, and gradually the exploration rate reduces and the exploitation rate increase.

Each iteration should check whether the particle has passed its previous record or not, and consequently, personal best should be updated. The condition for breaking a personal record in the minimization mode by the $i$ particle of the population is:

$Cost_i(t) < Cost_{i,best}(t)$ (2.26)

In addition, if a particle has left its record behind, it is also possible to leave the global record behind; thus, it should be checked and updated if necessary. The condition for breaking the global record by the $i^{th}$ particle of the population is (in the minimization mode):

$Cost_{i,best}(t) < Global\ Best\ Cost$ (2.27)

For implementing PSO algorithm, we should proceed in following steps:

1. Creating an initial population and evaluating it
2. Determining the best personal memories and the best collective memories
3. Update speed and position
4. If the stop conditions are not met, we go to step 2.
5. End

Several types of stopping conditions can be determined such as achieve an acceptable level of response, expiration of a certain number of repetitions or time, passing a certain number of repetitions or a specific time without observing a specific improvement in the result, check a certain number of responses. Figure 2.13 shows the flowchart of PSO Method. The PSO method does not depend on initial value. With any initial value it will converge to the optimum solution. Besides, this method is based on probability laws, then it is capable to search the undetermined and complicated spaces.

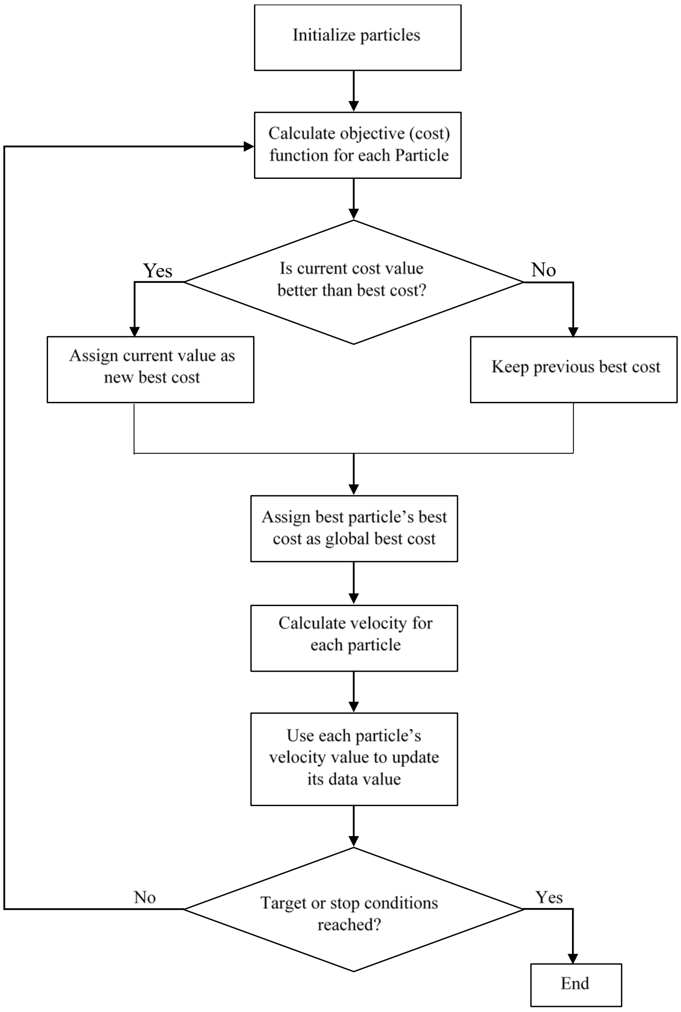


Figure 2.13. The PSO method flowchart

### 2.8.2 Hybrid PSO-GA Optimization Algorithm

The optimization method involves utilizing the PSO algorithm in conjunction with the simulation model to minimize waCOE, while ensuring compliance with constraints on renewable energy fraction $F_{RES}$. The GA-based reforming step is integrated to refine the positions of particles that fail to meet constraints until convergence is achieved or the stop condition is met. In this study, $F_{RES,min}$ is assumed to be 80%. This study addresses a nonlinear multidimensional optimization problem where the decision variables are the capacities of components across different scenarios, resulting in dimensions in the optimization space. Table 2.9 represents the identical concept for properties defined in the PSO method in this study. This optimization method follows a step-by-step process, as depicted in the flowchart shown in Figure 2.14. Initially, a population of particles is created, where each particle represents a specific configuration of RES components in one scenario. The capacity range of each component represents a search space that particles explore to find the optimal capacity of that component.

Table 2.9 Identical concept for properties defined in the PSO method

| PSO properties | Identical Concept |
|---|---|
| Particle position | Possible capacity of each component such as PV, wind, PTC, ORC component, electrolyzer, etc. |
| Particle cost | Weighted average cost of the energy in each position |
| Particle best cost | The minimum cost that the particle took so far |
| Global best cost | The minimum energy cost among all particles so far |
| Velocity | Direction that moves a particle from the previous position into the current position (Some in the direction of its current motion, A little towards its best memory, Some towards the best memory of all particles) |

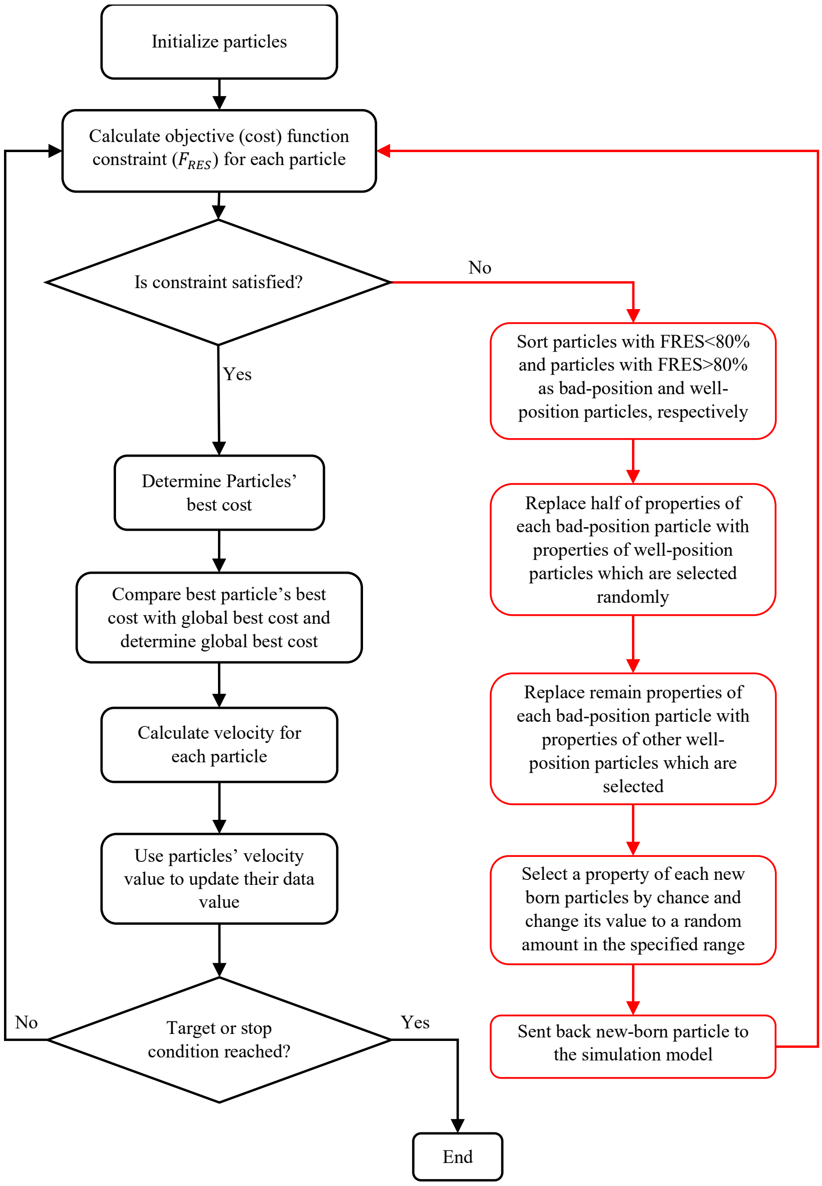


Figure 2.14. The PSO method flowchart and Reforming step utilizing the GA algorithm

In the first step, the initialized particles are sent into the simulation model, which calculates the $waCOE$ for each particle based on the configuration of RES components, as described in the previous sections. The $waCOE$s obtained from the simulation are then used by the PSO algorithm to determine the minimum $waCOE$, referred to as the global cost. In the next step, the data of the particles, including their positions, velocities, and previous best positions and costs, are updated using the velocity formula of the PSO algorithm. The updated particles are then sent back to the simulation for the next iteration. This process continues until a stop condition is met, such as reaching a maximum number of iterations or achieving a desired level of convergence. However, in this study, a constraint is introduced to avoid zero capacity for the storage system components while minimizing the cost of energy to have more realistic results. The constraint requires that $F_{RES}$ should be greater than the specified $F_{RES,min}$. The simulation method calculates $F_{RES}$ for each particle in addition to $waCOE$. If a particle does not satisfy the constraint, i.e., $F_{RES} < F_{RES,min}$, the position value of that particle is reformed using GA, as shown by the red line in Figure 2.14.

In the GA-based reforming step, first, particles with $F_{RES} < F_{RES,min}$ are identified as bad-position particles, while particles with $F_{RES} > F_{RES,min}$ are considered well-position particles. Then, half of the properties of each bad-position particle are replaced with the properties of one well-position particle selected randomly, and the remaining properties are replaced with the properties of another well-position particle, also randomly selected. Subsequently, a property of each newborn particle is selected by chance, and its value is changed by a random amount within the specified range. After these steps, the newborn particles are sent back to the simulation, and this cycle continues until all bad-position particles are modified to well-position particles. This GA-based reforming step helps improve the positions of the particles that do not meet the constraint, by exchanging properties with well-position particles and introducing random changes to explore the search space more effectively, which enhances the exploitation capability of the algorithm.

Overall, the optimization method in this study involves the use of PSO algorithm in conjunction with the simulation model to optimize the capacity of RES components based on the lowest $waCOE$, while also considering the constraint on $F_{RES}$. The GA-based reforming step is incorporated to improve the positions of particles that do not meet the constraint, and this process continues until convergence is achieved or the stop condition is met.

As mentioned before, this Study addresses a nonlinear multidimensional optimization problem. The decision variables in this problem are the capacities of components in different scenarios, which create dimensions in the optimization space. For instance, Scenarios #1 and #3 represent a 2D problem, Scenarios #2 and #4 represent a 4D problem, and Scenarios #5 and #6 represent 3D and 5D problems, respectively and finally Scenarios #7 represent an 8D problem, and Scenarios #8 represents 10D problem. Figure 2.15 represents the inputs, constraints, dimensions, and of the scenario #10. The proposed algorithm receives these processes them and finally release the optimized results as represented in this figure. Due to the multidimensional nature of the problem, particles in the PSO method need to explore a vast solution space. However, the PSO method converges quickly, and some areas of the solution space may be left unexplored. To address this issue, this study conducts multiple runs of the PSO algorithm, each starting from a different initial value or spot in the solution space. This approach ensures that particles explore the solution space from different perspectives, increasing the chances of finding the optimal solution. For this purpose, 50 runs of the PSO algorithm were performed, with each run consisting of 200 iterations. Figure 2.16, show 3 iterations of 3 different runs with 60 particles for scenario #5. As depicted from the figure, in each run, particles start to sweep the solution area from different spot, ensuring that whole solution space get investigated.

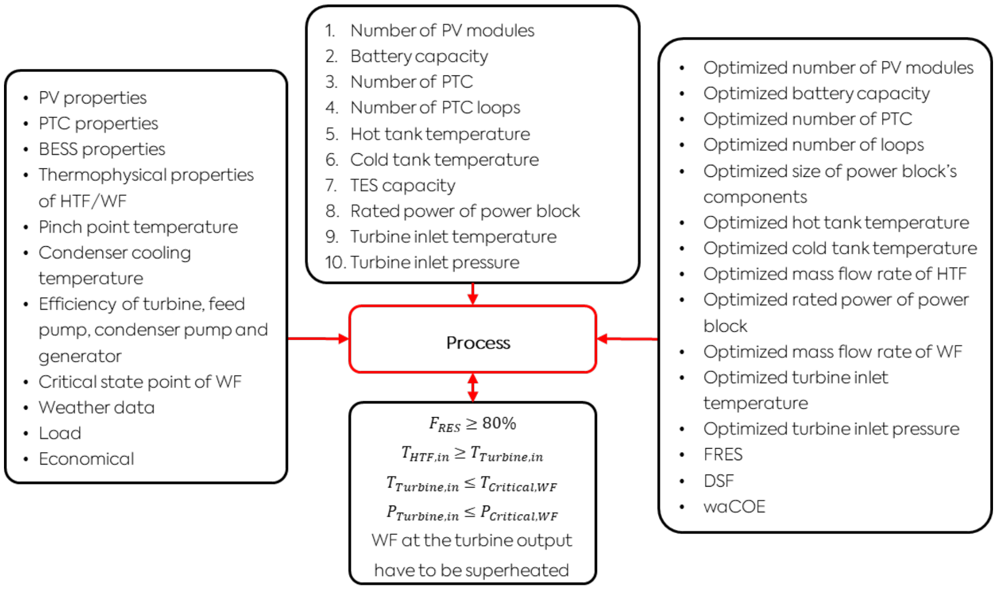


Figure 2.15. the inputs, constraints, dimensions, and of the scenario #10

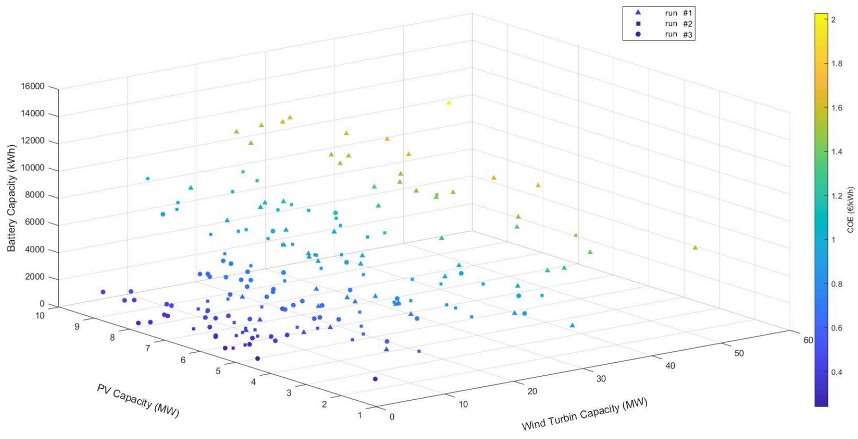

Figure 2.16. Optimization results of 3 iterations of 3 different runs with 60 particles for scenario #5

In terms of the PSO algorithm parameters i.e. inertia coefficient, personal, and global learning coefficients of 1, 0.25, and 1.75 are used, respectively. These coefficients determine the velocity update rule for particles in the PSO algorithm, controlling their movement and exploration of the solution space [92]

## 2.9 Case Study: Middle East Technical University Northern Cyprus Campus

The proposed methodology for sizing the hybrid renewable energy and ESS in this study is assessed using Middle East Technical University Northern Cyprus Campus as a case study. METU NCC is located in Güzelyurt, Northern Cyprus, at coordinates $35.183°\ N$ and $32.983°\ E$ with an altitude of approximately $120$ meters. Monthly average hourly global horizontal irradiation data for METU campus is shown in Figure 2.16, indicating that the campus has high solar resources with daily average of $4.93\ \mathrm{kWh/m^2}$. According to European Wind Classifications, this region is categorized as a moderately windy location, with annual average wind speeds of $2.8\ \mathrm{m/s}$ and a maximum speed of $5\ \mathrm{m/s}$ at a height of $10$ meters above the ground level. Monthly average hourly wind speed data measured at the height of $10$ meters is presented in Figure 2.17.

Figure 2.18 shows the yearly average hourly demand energy on the METU campus, which is provided by Kib-Tek, the local electricity authority. The load peak occurs in the mid of the day, aligning with the peak irradiation hours. However, the wind energy potential is higher in the afternoon. This suggests that a hybrid RES system combining PV and wind turbine technologies could be a favorable option to meet a large portion of the campus' energy demand. Since the maximum potential of solar and wind energy occurs at different intervals, they can complement each other in providing a reliable and sustainable energy supply for the campus.

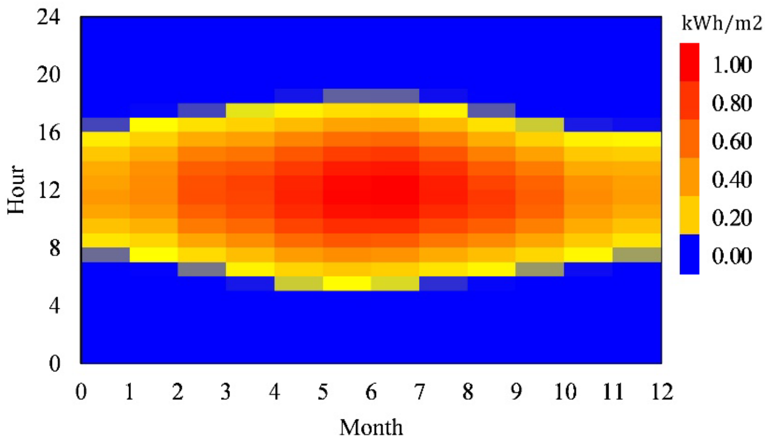


Figure 2.17. Monthly average hourly global horizontal irradiation on the campus.

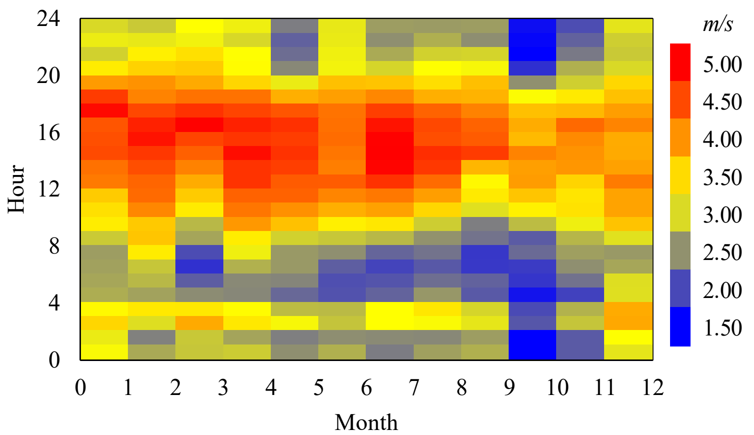


Figure 2.18. Monthly average hourly data for wind speed

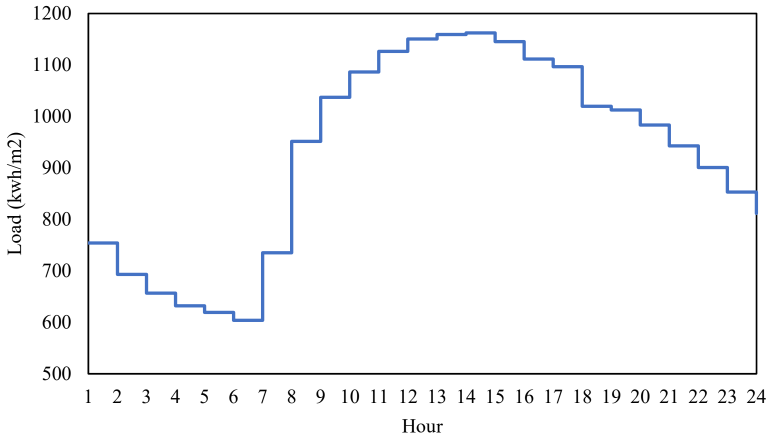


Figure 2.19. Yearly average hourly demand energy on the campus

# CHAPTER 3

# RESULTS AND DISCUSSION

In this study, the PV system is hybridized using two types of technologies. The first involves integrating the PV system with a different renewable energy source, namely wind turbines. The second combines the PV system with the same energy source, specifically a PTC/ORC. Wind energy serves as a complementary source to solar energy in the PV system, while the PTC-ORC system leverages the abundant solar energy available in the case study location, METU NCC in Northern Cyprus. To address the intermittency of RES and enhance their reliability, various ESS are utilized, including BESS, EFCS, and TES within the PTC system.

An economic optimization was conducted to determine the feasibility of the hybrid system and identify the more economical technology. This section first discusses the results of systems combining PV with wind energy and their integration with ESS. Subsequently, it analyzes the hybrid PV-PTC system. Finally, a comparison and conclusion of the results for both systems are presented. Thus, the scenarios included in the first and second sections are as follows:

**Hybrid PV-Wind System with Energy Storage**

- PV
- PV+BESS
- PV+EFCS
- Wind
- Wind + BESS
- Wind + EFCS
- PV + Wind + BESS
- PV + Wind + EFCS

**Hybrid PV-PTC System:**

- PTC
- PV+BESS+PTC

### 3.1 Hybrid PV-Wind System with Energy Storage

Table 3.1 presents the optimal capacities of the components for each scenario along with their corresponding $DSF$, $waCOE$, and $CoE$. To ensure the minimum $waCOE$ in each configuration with hybrid optimization method, a constraint of $F_{RES} > 80\%$ is imposed whenever it is applicable. The results in Table 3.1 show that the maximum $F_{RES}$ achieved by the PV system alone in this case study is $51.80\%$, which provides $41.22\%$ autonomy for optimal $waCOE$ of $0.2657$ €$/kWh$. When the PV system is coupled with BESS, the installed PV capacity decreases by about 39%, but $F_{RES}$ and $DSF$ of the system increase $28.2\%$ and $29{,}54\%$, respectively. Furthermore, this scenario achieves a lower $waCOE$ of 0.2392 €/kWh. Integrating PV with EFCS increases the installed capacity of the PV system from 7.65 MW to 7.89 MW. This configuration provides the $F_{RES}$ of $80\%$. However, due to the high capital cost of EFCS, the feasible minimum $waCOE$ is about $80\%$ more expensive than the PV system alone. The DSF of the system increased compared to the PV system alone means the autonomy of the system has been improved. Comparing the PV system coupled with BESS to the PV system alone and PV integrated with EFCS reveals that the PV+BESS configuration with an $F_{RES}$ of $80\%$ and higher $DSF$ and lower $waCOE$ is the best combination from both technical and economic perspectives.

In the case of considering only a wind turbine, the maximum available $F_{RES}$ for optimal $waCOE$ of $0.6052$€/kWh is $40\%$. The associated $DSF$ by this system is only $32.71\%$. Based on these values, the only-wind system is not a suitable renewable energy option for this region. Coupling the wind turbine with BESS improves the $F_{RES}$ and $DSF$, as well as the $waCOE$, compared to the wind-only and wind+EFCS configurations. Integrating the wind system with EFCS increases the $F_{RES}$ and $DSF$, it comes at the cost of higher $waCOE$. However, when comparing the wind turbine configurations to the integration of ESSs with a PV system, the wind turbine configurations are not an economical option. Despite the lower capital cost of the wind turbine compared to the PV system, the lower potential of wind energy compared to solar energy leads to a higher optimal $waCOE$. Therefore, in this region, the PV system coupled with ESSs is a more cost-effective and efficient renewable energy option than the wind turbine configurations.

Hybrid RESs, which combine multiple renewable energy sources, offer significant advantages over single-source systems, including increased energy efficiency, reduced intermittency, and enhanced system reliability. ESS are crucial for ensuring a reliable and stable energy supply in hybrid RES configurations. However, integrating an ESS adds costs, which must be weighed against the benefits of improved system performance. According to the data in Table 3.1, for the hybrid PV/wind system, the integration of a BESS resulted in an optimal waCOE when the wind capacity was zero, effectively transforming the system into a PV+BESS configuration. Despite the complementary nature of solar and wind energy in the studied region, the relatively weak wind energy potential led to the optimal solution excluding wind turbines to minimize energy costs. Conversely, coupling the hybrid PV/wind system with a EFCS included a $4\ MW$ wind turbine. This inclusion is driven by the high cost of HFCS technology, necessitating the use of wind energy to achieve the lowest possible waCOE. The integration of HFCS with the hybrid PV/wind system resulted in a waCOE of $0.4122\ €/kWh$. Although this scenario presents a cheaper waCOE compared to wind+ESS systems, it is still not economically feasible when compared to the PV system integrated with energy storage solutions.

These findings suggest that batteries are a more cost-effective energy storage option than hydrogen storage systems. However, it is important to note that hydrogen storage systems have other advantages. They are environmentally friendly, with minimal environmental impact, and hydrogen can be transported to the desired location when storage is low. Furthermore, as fuel cell and electrolyzer efficiencies improve, hydrogen storage systems may become more cost-effective and reliable in the future [6].

Table 3.1 The optimal capacities of the components for each scenario and their corresponding DSF, COE, and LCOE

| **Scenario** | **PV** | **PV+BESS** | **PV+EFCS** | **Wind** | **Wind + BESS** | **Wind + EFCS** | **PV + Wind + BESS** | **PV + Wind + EFCS** |
|---|---|---|---|---|---|---|---|---|
| **PV [MW]** | 7.65 | 4.67 | 7.89 | 26.00 | - | - | 4.67 | 5.11 |
| **Wind [MW]** | - | - | - | - | 19.69 | 22.14 | 0.00 | 4.00 |
| **EL [MW]** | - | - | 2.52 | - | - | 5.23 | - | 1.26 |
| **FC [MW]** | - | - | 1.61 | - | - | 1.97 | - | 1.25 |
| **$H_2$ Tank [kg]** | - | - | 835.50 | - | - | 11172 | - | 1755.3 |
| **Bat. [MWh]** | - | 8.21 | - | - | 37.54 | - | 8.21 | - |
| $F_{RES}$ **[%]** | 51.80 | 80.01 | 80.00 | 40.00 | 80.09 | 80.00 | 80.01 | 80.07 |
| $\boldsymbol{DSF}$ **[%]** | 41.22 | 70.76 | 52.07 | 32.71 | 78.12 | 59.97 | 70.76 | 57.82 |
| **waCOE [€/kWh]** | 0.2657 | 0.2392 | 0.4993 | 0.6052 | 0.8472 | 1.0255 | 0.2392 | 0.4122 |
| **CosE [€/kWh]** | 0.3176 | 0.2465 | 0.5716 | 1.1978 | 1.0057 | 1.2294 | 0.2465 | 0.4713 |

The daily demand load during one year and the contribution of RES, ESS, and grid in energy supply for each scenario are shown in Figure 3.1 to Figure 3.6. Comparing the systems integrated with PV to those coupled with wind turbines reveals that the configuration including PV is capable of supplying energy for the demand in a smoother state. Therefore, the configurations, including PV are more suitable for supplying base demand in this case study. The state of the energy in the ESS in the integration with wind turbine has intense fluctuation that can have an inverse effect on the lifespan of the ESS. When comparing the integrated hybrid system with EFCS with PV+EFCS, it can be depicted that the contribution of the storage systems is less in the hybrid system since the complementary solar and wind energy paves the difference and intermittency of the energy generation and demand load during a day and reduce the need for usage of expensive EFCS. Although the combination of the PV system with the wind turbine increases energy generation and reduces the need for ESS to supply the same amount of $F_{RES}$, it also increases the fluctuation in the supplied energy, which may not be desirable.

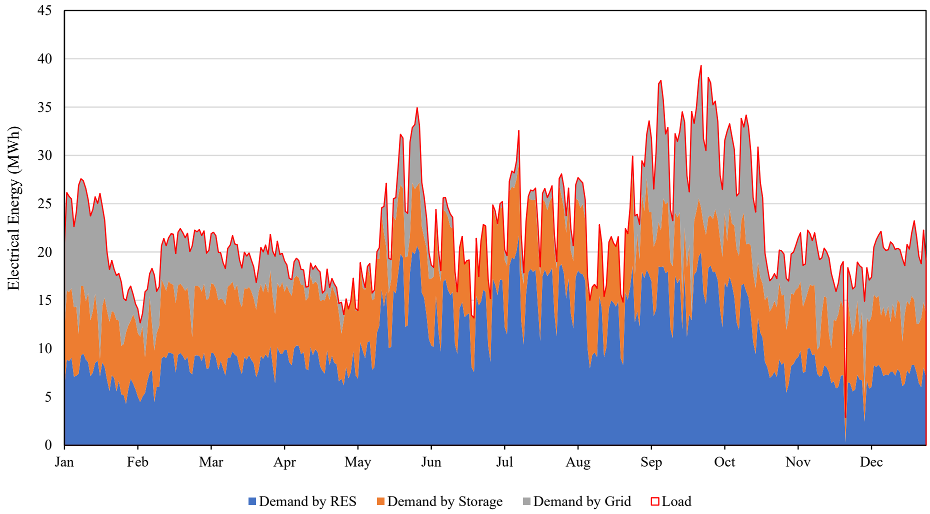


Figure 3.1. Daily demand load during one year and the contribution of RES, ESS, and grid in energy supply for PV+BESS

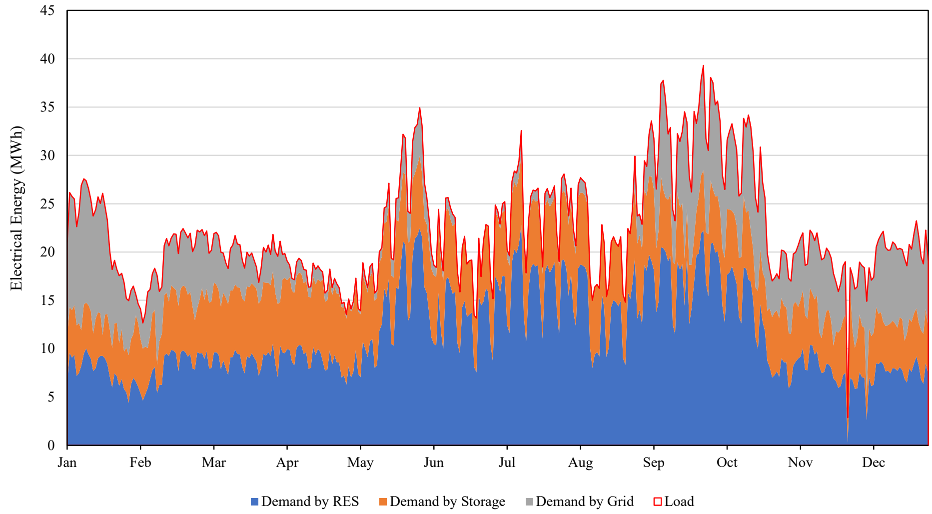


Figure 3.2. Daily demand load during one year and the contribution of RES, ESS, and grid in energy supply for PV+EFCS

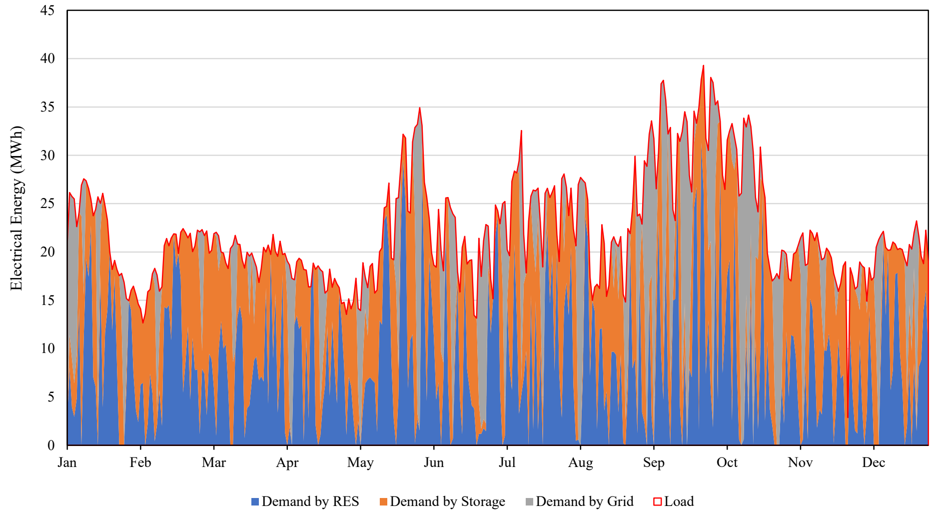


Figure 3.3. Daily demand load during one year and the contribution of RES, ESS, and grid in energy supply for Wind+BESS

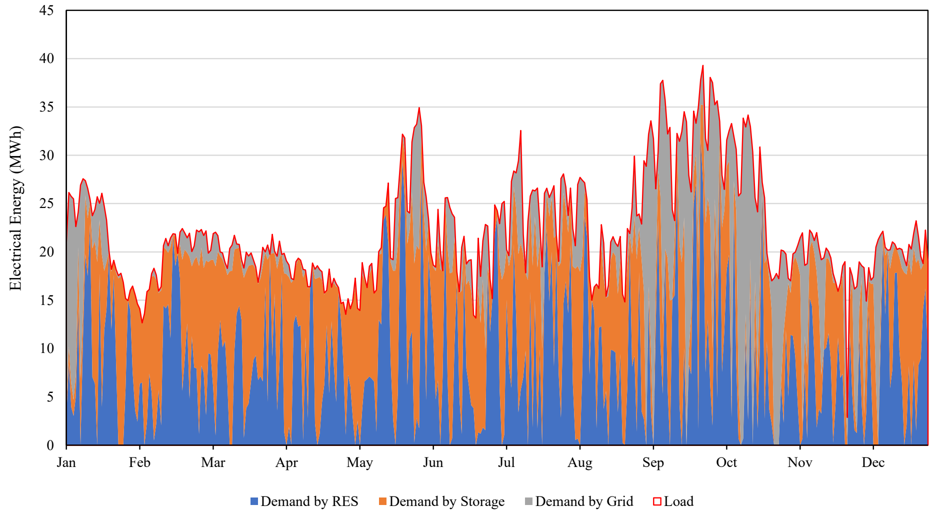


Figure 3.4. Daily demand load during one year and the contribution of RES, ESS, and grid in energy supply for Wind+EFCS

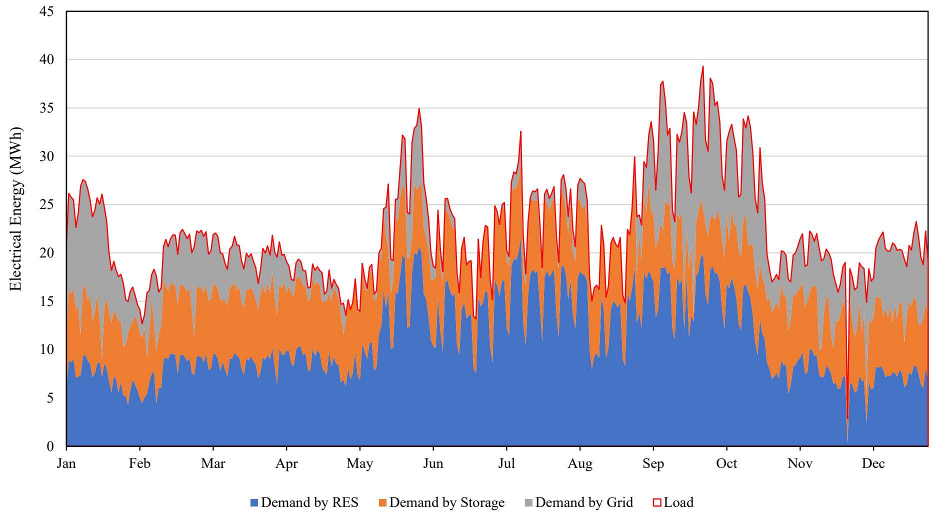


Figure 3.5. Daily demand load during one year and the contribution of RES, ESS, and grid in energy supply for PV+Wind+BESS

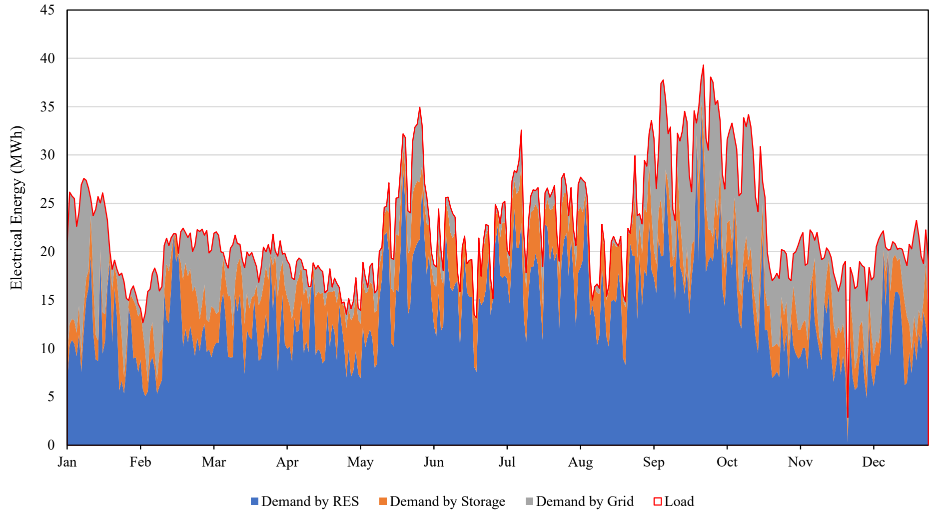


Figure 3.6. Daily demand load during one year and the contribution of RES, ESS, and grid in energy supply for PV+Wind+EFCS

The estimated energy expense in this study is consistent with the previous investigations, as shown in Table 3.2, which presents the $LCOE$ and $F_{RES}$ values for different systems from the recent literature over the last five years. Comparing the obtained $CosE$ value from Table 3.1 with the $LCOE$ values in Table 3.2 reveals that the obtained value falls within the acceptable range. It is noteworthy to mention that if conventional methods such as the $COE$ and $LCOE$ were utilized in the proposed study, the costs would likely appear more favorable. However, as previously stated, in the one-way tariff scheme, it is more realistic and logical to consider the utilization of the utilized renewable energy, rather than the total generated energy. This approach takes into account that the excess energy generated is often injected into the grid without any additional charge, and therefore does not generate any income for the producer. Notably, the $LCOE$ value in Table 3.2 for Reference [93] is associated with a study conducted as part of an EU Horizon 2020 project whose objective is to demonstrate the techno-economic feasibility of hydrogen-based energy storage solutions by installing demo systems in different regions. These cases provide valuable insights into the integration of the proposed systems with existing infrastructure in real-world settings, allowing for meaningful comparisons with results reported in the literature. It is worth mentioning that hybrid systems combining PV modules, wind turbines, and energy storage (such as, batteries and hydrogen storage) are being considered in various geographical regions. However, the optimal cost of these systems varies depending on factors such as solar radiation and wind speed patterns specific to each location. Therefore, the cost of these systems cannot be used as the sole indicator of their effectiveness, but rather reflects the potential of a particular location for implementing the proposed hybrid systems. This underscores the need for site-specific quantitative techno-economic analysis and optimal sizing to determine the feasibility and economic viability of hybrid systems in different locations of interest[6].

Table 3.2 Recently reported LCOE and $F_{RES}$ for different systems in the literature

| **Ref.** | **Pub. Year** | **System** | $F_{RES}$ **(%)** | **LCOE ($/kWh)** |
|---|---|---|---|---|
| **[6]** | 2023 | PV + BESS | => 95 | 0.1947 |
| | | PV + EFCS | => 95 | 1.5019 |
| | | Wind + BESS | => 95 | 0.3751 |
| | | Wind + EFCS | => 95 | 1.4902 |
| | | PV + Wind + BESS | => 95 | 0.1794 |
| | | PV + Wind + EFCS | => 95 | 0.7950 |
| **[16]** | 2022 | PV + Wind + BESS | 99.5 | 0.4 − 1.3 |
| | | PV + Wind + EFCS | 99.5 | 0.18 − 0.8 |
| **[11]** | 2021 | PV + BESS + EFCS | 100 | 0.4551 − 0.7216 |
| **[93]** | 2020 | PV + BESS + EFCS | 94.3 | 0.81 |
| | | PV + Wind + BESS + EFCS | 91.1 | 0.55 |
| **[15]** | 2019 | PV + EFCS | => 98 | 0.53 |
| | | Wind + EFCS | => 98 | 1.01 |
| | | PV + wind + Fuel cell | => 98 | 0.43 |

## 3.2 Hybrid PV-PTC System

Table 3.3 presents the optimal capacities of components for PTC and PV/PTC scenario alongside their corresponding waCOE and CosE. To ensure minimal waCOE within each configuration using the hybrid optimization method, a constraint of $F_{RES} \geq 80\%$ is applied when applicable.

In the case of a standalone PTC system, the maximum attainable $F_{RES}$ for an optimal waCOE of $0.3313$ €$/kWh$ is approximately $81.78\%$. To achieve this $F_{RES}$, the PTC requires 58 loops containing 18 modules, along with a hot tank capacity of $225\ kWh$. The power block is rated at $1403\ kW$ with a mass flow rate of $49\ kg/s$. While $F_{RES}$, increases $1{,}77\%$ compared to the PV+BESS system, the waCOE increases by 38.5%, indicating that the standalone PTC system is not as economically viable as the PV system within this microgrid context.

In contrast, the hybrid PV/PTC system demonstrates promising results. With an achievable $F_{RES}$ of 82%—comparable to that of the standalone PTC system—the waCOE is reduced to $0.2378$ €$/kWh$, making it a bit cheaper than the PV+BESS system. This hybrid solution leverages the advantages of both PV and PTC systems, emerging as the optimal choice among the proposed scenarios.

Examining the specifics of the hybrid system, the PV capacity is approximately 40% of PV capacity in the PV+BESS configuration. PTC modules in PV-PTC are organized into fewer loops (38 compared to 58 in the standalone PTC) and fewer number of modules in each loop (14 compared to 18 in the standalone PTC), resulting in a hot tank temperature $141°C$ less than that of the standalone PTC system. Notably, the cold tank temperature in the hybrid system is $99°C$ lower than in the standalone PTC. In the PTC-only system, the presence of a greater number of series modules in each loop results in a higher temperature differential between the hot and cold tanks compared to the hybrid system. Consequently, at the design condition, a greater amount of energy is transferred from the HTF to the working fluid.

Table 3.3 The optimal capacities of the components for each scenario and their corresponding waCOE and CosE

| Scenario | | PTC | PV+BESS+PTC |
|---|---|---|---|
| **PV** | **PV Cap. [MW]** | - | 1.76 |
| | **Bat. Cap [MWh]** | - | 0 |
| **PTC** | **# of Modules [-]** | 18 | 14 |
| | **# of Loops [-]** | 58 | 38 |
| **Heat Storage** | **Cap. [kWh]** | 225.34 | 121.53 |
| | $\boldsymbol{T_{Hst}}$ **[ºC]** | 516.36 | 375.12 |
| | $\boldsymbol{T_{Cst}}$ **[ºC]** | 388.93 | 290 |
| **ORC Design** | **Cap. [kW]** | 1402.8 | 774.65 |
| | $\boldsymbol{\dot{m}_{ORC}}$ **[kg/s]** | 48.96 | 26.67 |
| | $\boldsymbol{F_{RES}}$ **[%]** | 81.78 | 82.00 |
| | $\boldsymbol{DSF}$ **[%]** | 70.35 | 57.18 |
| | **waCOE [€/kWh]** | 0.3313 | 0.2378 |
| | **CosE [€/kWh]** | 0.3583 | 0.2439 |

Moreover, the hot tank capacity in the hybrid system is reduced to $121.53\ kWh$ compared to $225.34\ kWh$ in the standalone PTC, and the power block is optimized to a rated capacity of $774.65\ kW$ with a mass flow rate of $26.67\ kg/s$. These findings suggest that hybrid systems utilizing synergistic energy sources could be advantageous in microgrid contexts, particularly in regions with abundant solar energy potential. By combining PV and PTC systems, the need for expensive, short-lifespan BESS is mitigated, enhancing economic feasibility and environmental sustainability.

The DSF for each scenario is presented in Table 3.3. DSF is a critical metric for evaluating RESs, as it indicates the system's autonomy. The PTC system, and the hybrid PV system exhibit DSF values of 70.35%, and 57.18%, respectively. These figures highlight the significance of EES in ensuring system autonomy. The higher

DSF of the PV+BESS (70.76%) compared to the hybrid system underscores the pivotal role of batteries in maintaining autonomy. If PV panels were solely responsible for autonomy, the hybrid system would exhibit similar or higher DSF values, which is not the case. Additionally, the PTC system demonstrates greater autonomy than the hybrid system, attributable to the presence of thermal storage. As the thermal storage capacity decreases in the hybrid system, its autonomy correspondingly diminishes.

Figure 3.7 and Figure 3.8 illustrate the daily demand load throughout the year, along with the contribution of RES, ESS, and the grid in energy supply for each scenario. A notable observation emerges when comparing systems integrated with PTC to those incorporating PV modules, i.e., PV+BESS and PV+BESS+PTC: the only PTC system demonstrates the ability to meet the whole daily demand on more days. This distinction is discernible by examining the ranges where the RES curve intersects with the demand curve.

Given that the renewable resource remains consistent across all three scenarios, the energy supply patterns in all three scenarios, especially PV+PTC and PTC alone, may be assumed to be similar. However, the presence of a battery in the PV+BESS scenario reduces the number of days where the majority of demand is met by the grid, as evidenced by the minimum points in the RES system curves. In the PV+BESS scenario, the contribution of PV in meeting energy demand over one year is 49,93%, while the battery accounts for 30,10%, and the grid provides 19,90%. However, when PV is integrated with PTC, its contribution decreases to 35,19%, and the PTC's contribution becomes 46,81%, with the remaining 18% supplied by the grid. This comparison considering the energy cost, highlights that when a region has abundant solar resources, leveraging different technologies for exploiting that resource can overshadow the need for ESS technologies. In the scenario with only PTC, RES system supplies 81,78% of the demand, while the grid covers the remaining 18,22%.

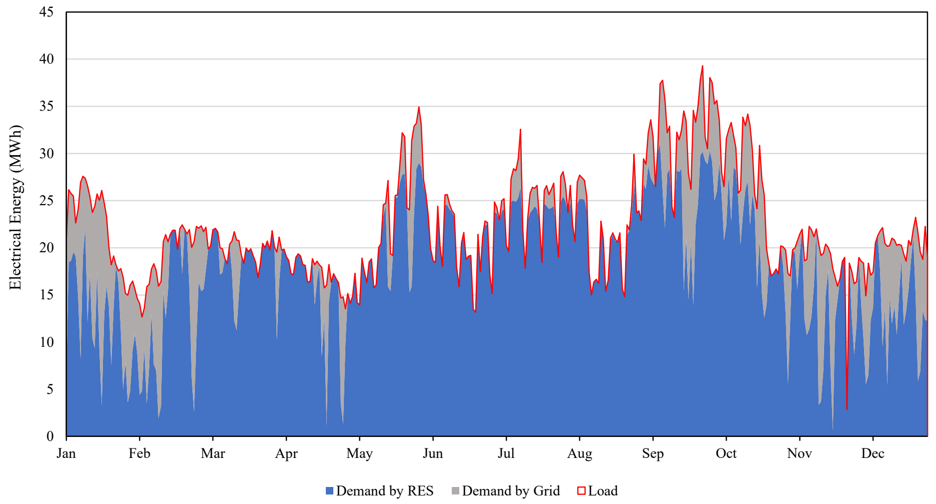


Figure 3.7. Daily demand load during one year and the contribution of RES, ESS, and grid in energy supply for PTC-ORC

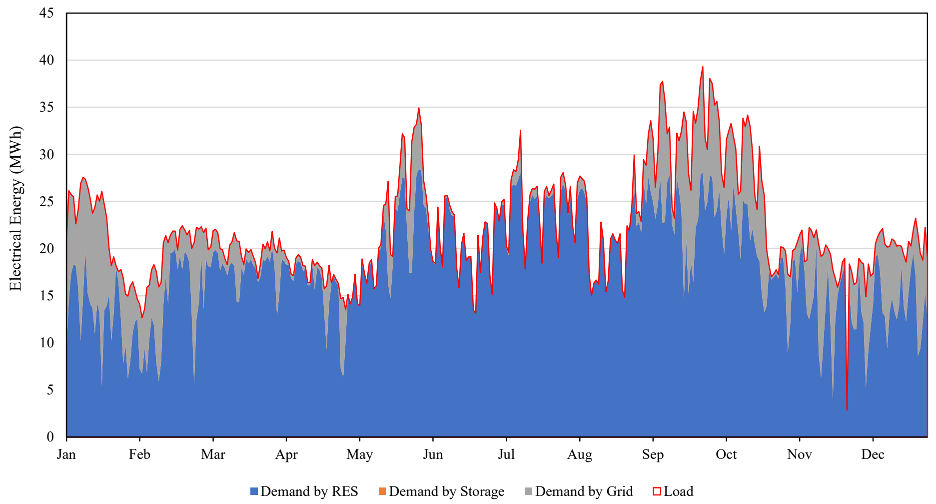


Figure 3.8. Daily demand load during one year and the contribution of RES, ESS, and grid in energy supply for PV+BESS+PTC-ORC

## 3.3 Comparison of the Hybrid PV-Wind System with Energy Storage with Hybrid PV-PTC System

Figure 3.9 illustrates the monthly variation of $F_{RES}$ for the scenarios in interest. It is clear from Figure 3.9 that the $F_{RES}$ values differ across the various scenarios and months. The fluctuation range for $F_{RES}$ lies within $50 - 100\%$ for all scenarios. This fluctuation is attributed to the seasonal changes in renewable resources as well as changes in demand. Notably, the systems that integrate with wind power exhibit their maximum $F_{RES}$ during the colder seasons, with a subsequent decrease during warmer seasons. Conversely, systems that couple with PV power display the opposite trend. It can thus be inferred that solar and wind energy are complementary not only on a daily basis but also seasonally.

The aim of the designed system is to achieve a $F_{RES}$ of 80%, therefore, it has been observed that none of the ESSs dominates the other over the course of the year. However, a notable difference can be observed in $DSF$ of the two ESSs, as shown in Figure 3.10. Across all scenarios, the system integrated with a battery is capable of achieving a higher $DSF$ compared to the system coupled with EFCS. On the other hand, the wind+EFCS system shows the lowest $DSF$, which also happens to have the highest $waCOE$ among all the scenarios, indicating that it is the least viable option. The autonomy of the hybrid PV-wind system is greater during the cold months compared to the PV-PTC system. However, this trend reverses during the hot season, with the PV-PTC system demonstrating greater autonomy. Therefore, when system autonomy is a critical factor, the type of renewable resource should be prioritized over the cost of energy. Similar to $F_{RES}$, $DSF$ of the scenarios varies throughout the year due to changes in renewable resources and demand.

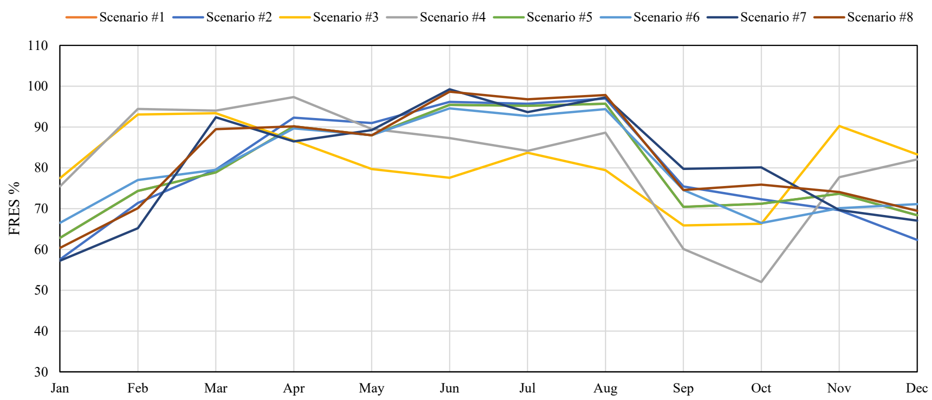


Figure 3.9. Monthly variation of the $F_{RES}$ for different scenarios

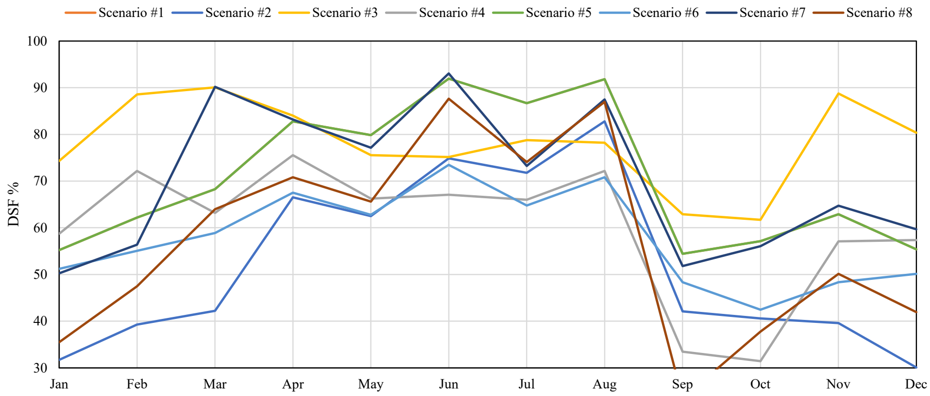


Figure 3.10. Monthly variation of the $DSF$ for different scenarios

Figure 3.11 displays the yearly contributions of RES, ESS, and the grid in meeting the energy demand, along with the amount of energy injected into the grid free of charge. The injected energy is a critical factor as it demonstrates the potential of the RES system to enhance the system's feasibility or reduce the $waCOE$ if sold to the grid. For example, in PV+EFCS, the injected energy represents approximately 65% of the demand by the grid, which is a significant amount. Selling this energy to the grid could reduce the $waCOE$. However, the systems integrated with wind turbines exhibit even higher levels of injected energy. The injected energy is 1.16 times of the demand met by RES + BESS in Scenario #3. In a one-way tariff system, this injected energy is considered wasted, resulting in a higher $waCOE$. Consequently, it can be inferred that wind turbines may not be the most suitable option for this region. On the other hand, systems including the PTC have the least injected energy to the grid among all proposed scenarios. Thus, in a one-way tariff structure, these hybrid systems appear to be more economically profitable since the wasted energy (injected to the grid for free) is reduced.

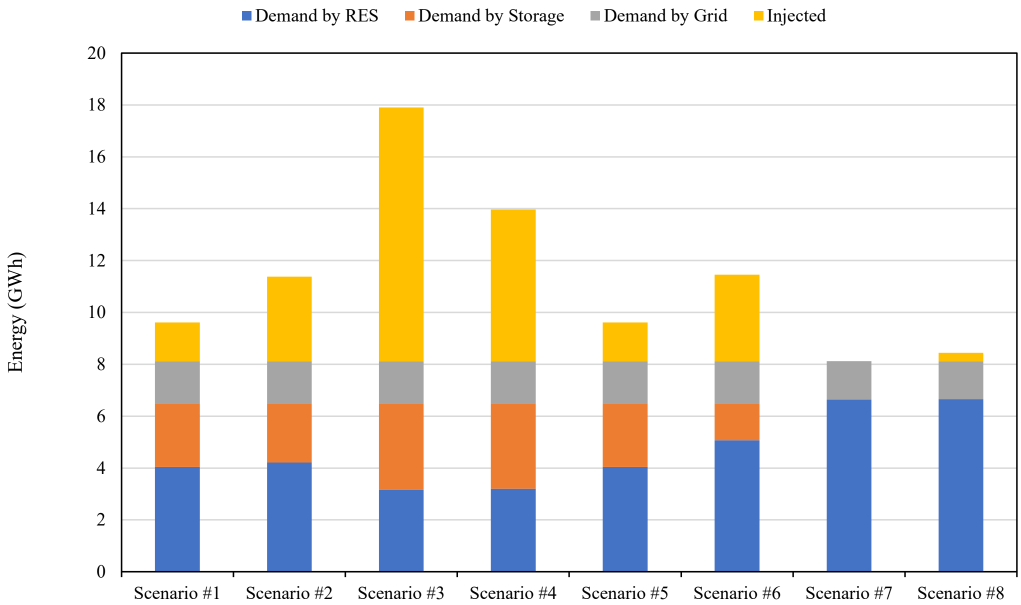


Figure 3.11. Yearly contribution of RES, ESS, and grid in meeting the energy demand, and the amount of energy injected to the grid free of charge for different scenarios

Table 3.4 represents the contribution of different components in initial cost of scenario 8, PV+PTC (the most economical feasible scenario). Within the power block, the turbine emerges as the most expensive component, followed by the heat exchangers, contributing significantly to the initial cost. While the contributions of PV and PTC in meeting energy demand may be comparable, the disparity in their contributions to the initial cost is significant. The PTC system's contribution to the initial cost, at 84%, is approximately five times that of PV, which accounts for 16%. Understanding each block's contribution to the initial cost is pivotal for assessing feasibility, as it directs attention to areas that require optimization. Improvements in the PTC system, particularly in thermal storage concentration, can significantly reduce energy costs. It's worth noting that the high cost associated with certain technologies reflects their status as emerging technologies. As these technologies mature, the cost hierarchy may undergo changes in the future.

Table 3.4 contribution of different components in initial cost of scenario 8

| Component | Initial cost [*1000 $] | Percentage of total initial cost [%] |
|---|---|---|
| **PV** | 2,721.90 | 16.17 |
| **Battery** | 0.00 | 0.00 |
| **PTC** | 7,008.89 | 41.64 |
| **HTF material** | 1,865.49 | 11.08 |
| **Two storage Tanks** | 3,779.74 | 22.46 |
| **Turbine** | 541.81 | 3.22 |
| **Generator** | 63.72 | 0.38 |
| **Evaporator** | 180.69 | 1.07 |
| **Condenser** | 203.93 | 1.21 |
| **Pump** | 41.62 | 0.25 |
| **Land and site development cost** | 150.19 | 0.89 |
| **Civil works cost** | 130.60 | 0.78 |
| **Miscellaneous cost** | 141.76 | 0.84 |

The Figures 3.12 to 3.15 represent the sensitivity of the waCOE and $F_{RES}$ to the different component capacities within the hybrid PV-PTC integrated with ORC system. This analysis aims to identify the most effective components for optimizing both the cost of energy and the renewable energy fraction. Examining the impacts of varying key parameters, such as hot storage temperature ($T_{Hst}$), ORC capacity, number of PTC modules and loops, thermal energy storage (TES) capacity and PV capacity (when the other parameters et to optimized value) gain valuable insights into improving the system's performance and cost-efficiency.

Considering Figure 3.12a, increasing the number of modules significantly enhances $F_{RES}$ while maintaining a relatively stable waCOE at first steps, making it a viable strategy for improving sustainability without incurring additional costs in this range. However, after a specific point (about 10 Modules) the waCOE start to increase. It is due to the fact that the output temperature is set to be constant therefore the mass flow of the HTF must be increased maintain the energy balance, however, in one point, this high amount of heated mass would be unfavorable due to the limitation of mass amount could be stored in hot and cold storage tank. Similarly, increasing the number of loops raises both waCOE and FRES, highlighting the need to balance the number of loops to optimize cost-effectiveness and renewable contribution, Figure 3.12b.

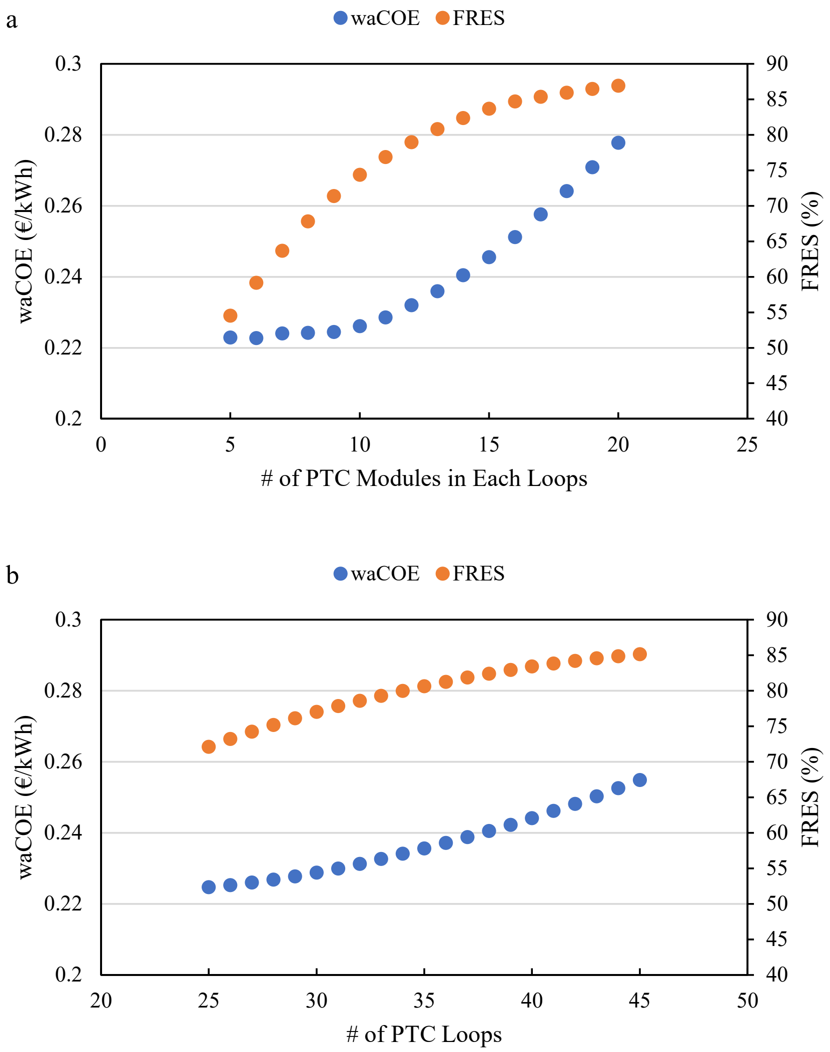


Figure 3.12. Sensitivity of waCOE and $F_{RES}$ to a) the number of PTC modules and b) number of loops in scenario #10

When examining the hot storage temperature ($T_{Hst}$), Figure 3.13a, it is evident that as $T_{Hst}$ increases, the waCOE decreases before stabilizing, while the $F_{RES}$ increases before becoming relatively constant. This suggests that increasing $T_{Hst}$

initially makes the system more cost-effective and significantly boosting the renewable fraction. In contrast, variations in TES capacity show no significant impact on $F_{RES}$, but it increases the waCOE in a modest way, suggesting TES capacity is not a major factor in overall performance, in this range, Figure 3.13b.

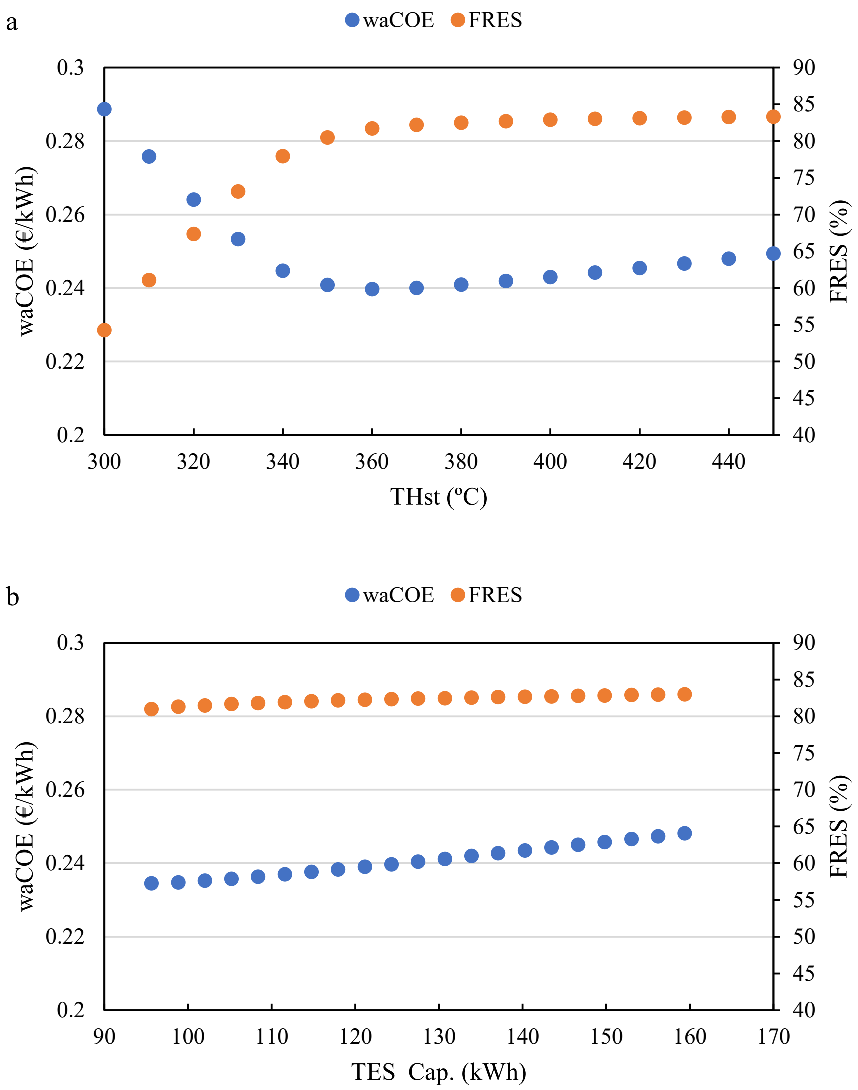


Figure 3.13. Sensitivity of waCOE and $F_{RES}$ to the a) hot storage temperature and b) TES capacity in scenario #10

Considering the Figure 3.14, changes in ORC capacity show no impact on either waCOE or $F_{RES}$, indicating that ORC capacity is not a critical factor within the tested range.

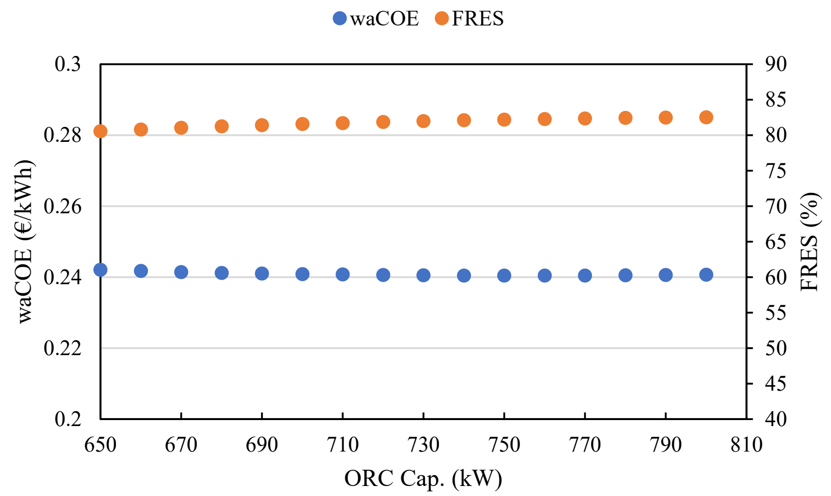


Figure 3.14. Sensitivity of waCOE and $F_{RES}$ to the ORC capacity in scenario #10

Finally, Figure 3.15 indicates that higher PV capacity boosts $F_{RES}$ while keeping the waCOE relatively stable; since in the hybrid PV-PTC the amount of the demand met by PV is low (i.e. there is more capacity to cover the demand using PV), making it an effective strategy for enhancing sustainability.

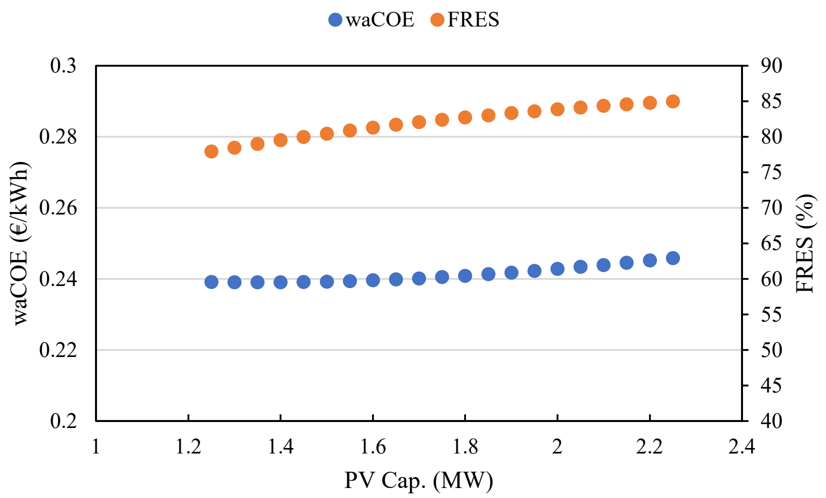


Figure 3.15. Sensitivity of waCOE and $F_{RES}$ to the capacity of PV power plant in scenario #10

Overall, the most effective components for increasing $F_{RES}$ are the number of PTC modules and PV capacity, while $T_{Hst}$ has also significant effect on reducing waCOE initially.

# CHAPTER 4

# CONCLUSIONS

In this study, the PV system is examined in integration with various ESS, including batteries and fuel cells. Additionally, it is assessed in hybrid systems that incorporate wind turbines and PTC systems to meet the electricity demand of the METU NCC campus. The PTC/ORC systems are also evaluated independently. As a result, eight scenarios representing different integrated systems are investigated including Scenario#1: PV+BESS, Scenario#2: PV+EFC, Scenario#3: Wind+BESS, Scenario#4: Wind+EFCS, Scenario#5: PV+Wind+BESS, Scenario#6: PV+Wind+EFCS, Scenario#7: PTC, Scenario#8: PV+BESS+PTC.

By employing PSO and GA, the study aims to minimize the waCOE while maintaining a specific renewable energy fraction. The optimization method involves utilizing the PSO algorithm in conjunction with the simulation model to minimize waCOE, while ensuring compliance with constraints on renewable energy fraction $F_{RES}$. The GA-based reforming step is integrated to refine the positions of particles that fail to meet constraints until convergence is achieved or the stop condition is met. In this study, $F_{RES,min}$ is assumed to be 80%. This study addresses a nonlinear multidimensional optimization problem where the decision variables are the capacities of components across different scenarios, resulting in dimensions in the optimization space. The optimization process addresses the capacities of all critical components, including the PV panels, wind turbine, Battery, electrolyzer, hydrogen tank, fuel cell, trough collector, thermal storage tanks, turbine, evaporator, heat exchangers, condenser, and pump. Additionally, it optimizes the flow rates for the heat transfer fluid and working fluid under realistic operating conditions, considering the fluctuating efficiency of the ORC and the impact of partial load on turbine efficiency, resulting in a complex and nonlinear optimization problem. A case study on a university campus located on a Mediterranean island, which relies on imported fossil fuels for electricity, reveals that a PV-PTC hybrid system with a $14 * 38\ MW$ trough collector, a $1.76\ MW$ PV, $121.53\ kWh$ heat storage, and an $774.65\ kW$ ORC achieves the lowest waCOE at $0.2378\ €/kWh$. This system also provides a DSF of $57.18\%$ with an $F_{RES}$ of $82\%$. On the contrary, the wind+EFCS system is the least economical scenario due to the low potential of wind energy compared to solar energy in this region, as well as the high cost of EFCS technology. The injected energy is a critical factor as it demonstrates the potential of the RES system to enhance the system's feasibility or reduce the $waCOE$ if sold to the grid. The systems integrated with wind turbines exhibit highest levels of injected energy. On the other hand, systems including the PTC have the least injected energy to the grid among all proposed scenarios. Thus, in a one-way tariff structure, these hybrid systems appear to be more economically profitable since the wasted energy (injected to the grid for free) is minimized.

The economic analysis indicates that in PV-PTC, the turbine is the most expensive component within the power block, followed by the heat exchangers. Although PV and PTC contribute similarly to meeting energy demand, their initial costs differ significantly, with the PTC system accounting for $84\%$ of the initial cost, approximately five times more than PV at $16\%$. This understanding is crucial for assessing feasibility and directing optimization efforts, particularly in improving the PTC system and its thermal storage. The high costs of certain technologies reflect their emerging status, which may change as they mature. Overall, this study demonstrates that hybrid systems integrating PV and PTC/ORC are highly effective in regions with abundant solar energy. Such systems significantly enhance the contribution of renewable energy to microgrid demands, providing reliable and efficient energy solutions. The research paves the way for the broader adoption of hybrid renewable systems, ensuring sustainable and independent energy solutions for microgrids. This novel methodology highlights the potential for optimizing complex hybrid energy systems, promoting a resilient and economical approach to renewable energy integration.

Future work will focus on several key areas to further enhance the viability and efficiency of hybrid PV-PTC systems. Firstly, assessing the technical and economic efficiency improvements of PTC-ORC systems incorporating reheat or regenerative-ORC configurations will be pivotal. Additionally, evaluating the impact of dynamic dispatching strategies on the economic and theoretical efficiency of PTC-ORC systems will provide deeper insights into operational optimization. The transient analysis for the system could be done for getting valuable insights regarding the system performance and lifetime especially in systems including BESS. Another significant area of development involves creating a modified PSO-GA-EES approach to increase the interaction velocity between MATLAB and EES, thereby reducing solution times. Lastly, the development of machine learning optimization methods for the precise sizing of hybrid PTC-PV power plants will offer a cutting-edge approach to system design. These future research directions will contribute substantially to the advancement of hybrid renewable energy systems, ensuring they are more efficient, cost-effective, and adaptable to varying energy demands

## REFERENCES


[1] Khan, M.W., et al., Optimal energy management and control aspects of distributed microgrid using multi-agent systems. Sustainable Cities and Society, 2019. 44: p. 855-870.

[2] Guangul, F.M. and G.T. Chala. Solar energy as renewable energy source: SWOT analysis. in 2019 4th MEC international conference on big data and smart city (ICBDSC). 2019. IEEE.

[3] Weldekidan, H., V. Strezov, and G. Town, Review of solar energy for biofuel extraction. Renewable and Sustainable Energy Reviews, 2018. 88: p. 184-192.

[4] Kabir, E., et al., Solar energy: Potential and future prospects. Renewable and Sustainable Energy Reviews, 2018. 82: p. 894-900.

[5] Zhao, Z., M.T. Arif, and A.M. Oo, Solar thermal energy with molten-salt storage for residential heating application. Energy Procedia, 2017. 110: p. 243-249.

[6] Ngouleu, C.A.W., et al., Techno-economic analysis and optimal sizing of a battery-based and hydrogen-based standalone photovoltaic/wind hybrid system for rural electrification in Cameroon based on meta-heuristic techniques. Energy Conversion and Management, 2023. 280: p. 116794.

[7] Fodhil, F., A. Hamidat, and O. Nadjemi, Potential, optimization and sensitivity analysis of photovoltaic-diesel-battery hybrid energy system for rural electrification in Algeria. Energy, 2019. 169: p. 613-624.

[8] Upadhyay, S. and M. Sharma, A review on configurations, control and sizing methodologies of hybrid energy systems. Renewable and Sustainable Energy Reviews, 2014. 38: p. 47-63.

[9] Medghalchi, Z. and O. Taylan, A novel hybrid optimization framework for sizing renewable energy systems integrated with energy storage systems with solar photovoltaics, wind, battery and electrolyzer-fuel cell. Energy Conversion and Management, 2023. 294: p. 117594.

[10] Kerdphol, T., et al., Optimization of a battery energy storage system using particle swarm optimization for stand-alone microgrids. International Journal of Electrical Power & Energy Systems, 2016. 81: p. 32-39.

[11] Mah, A.X.Y., et al., Optimization of a standalone photovoltaic-based microgrid with electrical and hydrogen loads. Energy, 2021. 235: p. 121218.

[12] Makhdoomi, S. and A. Askarzadeh, Techno-enviro-economic feasibility assessment of an off-grid hybrid energy system with/without solar tracker considering pumped hydro storage and battery. IET Renewable Power Generation, 2023. 17(5): p. 1194-1211.

[13] Singh, S., P. Chauhan, and N. Singh, Capacity optimization of grid connected solar/fuel cell energy system using hybrid ABC-PSO algorithm. International Journal of Hydrogen Energy, 2020. 45(16): p. 10070-10088.

[14] Elnozahy, A., H. Ramadan, and F.K. Abo-Elyousr, Efficient metaheuristic Utopia-based multi-objective solutions of optimal battery-mix storage for microgrids. Journal of Cleaner Production, 2021. 303: p. 127038.

[15] Samy, M., S. Barakat, and H. Ramadan, Techno-economic analysis for rustic electrification in Egypt using multi-source renewable energy based on PV/wind/FC. International Journal of Hydrogen Energy, 2020. 45(20): p. 11471-11483.

[16] Shahid, Z., et al., Techno-economic feasibility analysis of Renewable-fed Power-to-Power (P2P) systems for small French islands. Energy Conversion and Management, 2022. 255: p. 115368.

[17] Aziz, A.S., et al., Feasibility analysis of grid-connected and islanded operation of a solar PV microgrid system: A case study of Iraq. Energy, 2020. 191: p. 116591.

[18] Alramlawi, M. and P. Li, Design optimization of a residential PV-battery microgrid with a detailed battery lifetime estimation model. IEEE Transactions on Industry Applications, 2020. 56(2).

[19] Dawood, F., G. Shafiullah, and M. Anda, Stand-alone microgrid with 100% renewable energy: A case study with hybrid solar PV-battery-hydrogen. Sustainability, 2020. 12(5): p. 2047.

[20] Yuan, H., et al., Research on the optimal configuration of photovoltaic and energy storage in rural microgrid. Energy Reports, 2022. 8: p. 1285-1293.

[21] Singh, S.K., A.K. Tiwari, and H. Paliwal, Thermo-economic assessment of hybrid Kalina cycle and organic Rankine cycle system using a parabolic

trough collector solar field. Thermal Science and Engineering Progress, 2023. 46: p. 102132.

[22] Ata, S., et al., Which power cycle is the best fit for parabolic trough solar collectors? A comparative and comprehensive case study for six sub-configurations of the three main cycles. Energy Conversion and Management, 2023. 291: p. 117338.

[23] Alshammari, F., N.B. Khedher, and L.B. Said, Development of an automated design and off-design radial turbine model for solar organic Rankine cycle coupled to a parabolic trough solar collector. Applied Thermal Engineering, 2023. 230: p. 120677.

[24] Martin, A., et al., Solar Thermal Collector System with Parabolic Collector for Applications in Organic Rankine Cycle: Design, Manufacturing and Testing. Journal of Advanced Research in Fluid Mechanics and Thermal Sciences, 2023. 104(2): p. 127-138.

[25] Desai, N.B. and S. Bandyopadhyay, Optimization of concentrating solar thermal power plant based on parabolic trough collector. Journal of Cleaner Production, 2015. 89: p. 262-271.

[26] Cabello, J., et al., Optimization of the size of a solar thermal electricity plant by means of genetic algorithms. Renewable Energy, 2011. 36(11): p. 3146-3153.

[27] Quoilin, S., et al., Performance and design optimization of a low-cost solar organic Rankine cycle for remote power generation. Solar energy, 2011. 85(5): p. 955-966.

[28] Yasmeen, R., et al., The role of wind energy towards sustainable development in top-16 wind energy consumer countries: Evidence from STIRPAT model. Gondwana Research, 2023. 121: p. 56-71.

[29] Rekik, S. and S. El Alimi, Optimal wind-solar site selection using a GIS-AHP based approach: A case of Tunisia. Energy Conversion and Management: X, 2023. 18: p. 100355.

[30] Baseer, M., et al., GIS-based site suitability analysis for wind farm development in Saudi Arabia. Energy, 2017. 141: p. 1166-1176.

[31] Imam, A.A., A. Abusorrah, and M. Marzband, Potentials and opportunities of solar PV and wind energy sources in Saudi Arabia: Land suitability,

techno-socio-economic feasibility, and future variability. Results in Engineering, 2024. 21: p. 101785.

[32] Solyali, D. and M.A. Redfern. Case study of Cyprus: Wind energy or solar power. in 11th International Scientific Conference on Electric Power Engineering. 2010.

[33] İlkan, M., E. Erdil, and F. Egelioglu, Renewable energy resources as an alternative to modify the load curve in Northern Cyprus. Energy, 2005. 30(5): p. 555-572.

[34] N'guessan, S.A., et al., Optimal sizing of a wind, fuel cell, electrolyzer, battery and supercapacitor system for off-grid applications. International Journal of Hydrogen Energy, 2020. 45(8): p. 5512-5525.

[35] Fokaides, P.A., et al., Promotion of wind energy in isolated energy systems: the case of the Orites wind farm. Clean Technologies and Environmental Policy, 2014. 16: p. 477-488.

[36] Bhandari, B., et al., A novel off-grid hybrid power system comprised of solar photovoltaic, wind, and hydro energy sources. Applied Energy, 2014. 133: p. 236-242.

[37] Divya, K.C. and J. Østergaard, Battery energy storage technology for power systems—An overview. Electric power systems research, 2009. 79(4): p. 511-520.

[38] Ma, T., et al., Technical feasibility study on a standalone hybrid solar-wind system with pumped hydro storage for a remote island in Hong Kong. Renewable energy, 2014. 69: p. 7-15.

[39] Apribowo, C.H.B., et al., Optimal sizing and placement of battery energy storage system for maximum variable renewable energy penetration considering demand response flexibility: A case in Lombok power system, Indonesia. Energy Conversion and Management: X, 2024: p. 100620.

[40] Rayit, N.S., J.I. Chowdhury, and N. Balta-Ozkan, Techno-economic optimisation of battery storage for grid-level energy services using curtailed energy from wind. Journal of Energy Storage, 2021. 39: p. 102641.

[41] Devrim, Y. and L. Bilir, Performance investigation of a wind turbine–solar photovoltaic panels–fuel cell hybrid system installed at İncek region–Ankara, Turkey. Energy Conversion and Management, 2016. 126: p. 759-766.

[42] Kim, D.K., et al., Evaluation of energy storage technologies for efficient usage of wind power in the far-eastern region: A techno-economic analysis. Journal of Energy Storage, 2021. 39: p. 102595.

[43] Aguilar-Jiménez, J., et al., Techno-economic analysis of a hybrid PV-CSP system with thermal energy storage applied to isolated microgrids. Solar Energy, 2018. 174: p. 55-65.

[44] Starke, A.R., et al., Assessing the performance of hybrid CSP+ PV plants in northern Chile. Solar Energy, 2016. 138: p. 88-97.

[45] Sumayli, H., et al., Integrated CSP-PV hybrid solar power plant for two cities in Saudi Arabia. Case Studies in Thermal Engineering, 2023. 44: p. 102835.

[46] Pilotti, L., et al., Simultaneous design and operational optimization of hybrid CSP-PV plants. Applied Energy, 2023. 331: p. 120369.

[47] Parrado, C., et al., 2050 LCOE (Levelized Cost of Energy) projection for a hybrid PV (photovoltaic)-CSP (concentrated solar power) plant in the Atacama Desert, Chile. Energy, 2016. 94: p. 422-430.

[48] Furlan, G. and F. You, Robust Design of Hybrid Solar Power Systems: Sustainable Integration of Concentrated Solar Power and Photovoltaic Technologies. Advances in Applied Energy, 2024: p. 100164.

[49] Ghirardi, E., et al., The optimal share of PV and CSP for highly renewable power systems in the GCC region. Renewable Energy, 2021. 179: p. 1990-2003.

[50] Haddad, A., et al., An investigation on coupling fuel cell, wind turbine and PV as green to green system. International Journal of Hydrogen Energy, 2022.

[51] Van, L.P., et al., An improved state machine-based energy management strategy for renewable energy microgrid with hydrogen storage system. Energy Reports, 2023. 9: p. 194-201.

[52] Javed, M.S., et al., Hybrid pumped hydro and battery storage for renewable energy based power supply system. Applied Energy, 2020. 257: p. 114026.

[53] Shayeghi, H., et al., A survey on microgrid energy management considering flexible energy sources. Energies, 2019. 12(11): p. 2156.

[54] Adefarati, T., et al., Analysis and optimisation of a diesel-PV-wind-electric storage system for a standalone power solution. IET Renewable Power Generation, 2020. 14(19): p. 4053-4062.

[55] Akram, U., M. Khalid, and S. Shafiq, Optimal sizing of a wind/solar/battery hybrid grid-connected microgrid system. IET Renewable Power Generation, 2018. 12(1): p. 72-80.

[56] Ghaffari, A. and A. Askarzadeh, Design optimization of a hybrid system subject to reliability level and renewable energy penetration. Energy, 2020. 193: p. 116754.

[57] Maheri, A., I. Unsal, and O. Mahian, Multiobjective optimisation of hybrid wind-PV-battery-fuel cell-electrolyser-diesel systems: An integrated configuration-size formulation approach. Energy, 2022. 241: p. 122825.

[58] Akhavan Shams, S. and R. Ahmadi, Dynamic optimization of solar-wind hybrid system connected to electrical battery or hydrogen as an energy storage system. International Journal of Energy Research, 2021. 45(7): p. 10630-10654.

[59] Vaderobli, A., D. Parikh, and U. Diwekar, Optimization under uncertainty to reduce the cost of energy for parabolic trough solar power plants for different weather conditions. Energies, 2020. 13(12): p. 3131.

[60] Garg, P., M.S. Orosz, and P. Kumar, Thermo-economic evaluation of ORCs for various working fluids. Applied Thermal Engineering, 2016. 109: p. 841-853.

[61] Esfahani, M.N., A.H. Aghdam, and A. Refahi, Energy, exergy, exergoeconomic, exergoenvironmental (4E) assesment, sensitivity analysis and multi-objective optimization of a PTC–tehran climate data case study. Journal of Cleaner Production, 2023. 415: p. 137821.

[62] Lou, J., et al., Power load analysis and configuration optimization of solar thermal-PV hybrid microgrid based on building. Energy, 2024. 289: p. 129963.

[63] HassanzadehFard, H., et al., Design and optimum energy management of a hybrid renewable energy system based on efficient various hydrogen production. International Journal of Hydrogen Energy, 2020. 45(55): p. 30113-30128.

[64] Moradi, M.H. and M. Abedini, A combination of genetic algorithm and particle swarm optimization for optimal DG location and sizing in distribution systems. International Journal of Electrical Power & Energy Systems, 2012. 34(1): p. 66-74.

[65] Musa, H. and S. Ibrahim, A review of particle swarm optimization (PSO) algorithms for optimal distributed generation placement. International Journal of Energy and Power Engineering, 2015. 4(4): p. 232-239.

[66] García-Triviño, P., et al., Optimized operation combining costs, efficiency and lifetime of a hybrid renewable energy system with energy storage by battery and hydrogen in grid-connected applications. International Journal of Hydrogen Energy, 2016. 41(48): p. 23132-23144.

[67] Sharafi, M. and T.Y. ELMekkawy, Multi-objective optimal design of hybrid renewable energy systems using PSO-simulation based approach. Renewable energy, 2014. 68: p. 67-79.

[68] Askarzadeh, A., Solution for sizing a PV/diesel HPGS for isolated sites. IET renewable power generation, 2017. 11(1): p. 143-151.

[69] Chen, K., et al., Optimized Demand-Side Day-Ahead Generation Scheduling Model for a Wind–Photovoltaic–Energy Storage Hydrogen Production System. ACS omega, 2022. 7(47): p. 43036-43044.

[70] Ziari, I., et al. Optimal allocation and sizing of DGs in distribution networks. in IEEE PES general meeting. 2010. IEEE.

[71] Innocente, M.S. and J. Sienz, Constraint-handling techniques for particle swarm optimization algorithms. arXiv preprint arXiv:2101.10933, 2021.

[72] Bakhtiari, H. and R.A. Naghizadeh, Multi-criteria optimal sizing of hybrid renewable energy systems including wind, photovoltaic, battery, and hydrogen storage with ε-constraint method. IET renewable power generation, 2018. 12(8): p. 883-892.

[73] Al-Ghussain, L., et al., Sizing renewable energy systems with energy storage systems in microgrids for maximum cost-efficient utilization of renewable energy resources. Sustainable Cities and Society, 2020. 55: p. 102059.

[74] Meuris, M., et al., Managing PV power injection and storage, enabling a larger direct consumption of renewable energy: A case study for the Belgian electricity system. Progress in Photovoltaics: Research and Applications, 2019. 27(11): p. 905-917.

[75] Duffie, J.A., W.A. Beckman, and N. Blair, Solar engineering of thermal processes, photovoltaics and wind. 2020: John Wiley & Sons.

[76] Technical specification of the AXIPower-AC-250P/156-60S PV module http://www.solariaenergy.it/wp-content/uploads/2013/08/Axitec_DB_60zlg_poly_power_MiE_GB.pdf.

[77] Kalogirou, S.A., Solar energy engineering: processes and systems. 2013: Academic press.

[78] Manwell, J.F., J.G. McGowan, and A.L. Rogers, Wind energy explained: theory, design and application. 2010: John Wiley & Sons.

[79] V90-2.0 MW™ IEC IIA/IEC S Technical Sheet https://www.vestas.com/en/pages/backup-2-mw-platform/V90-2-0-MW.

[80] Lüpfert, E., et al. Euro Trough collector qualification complete-performance test results from PSA. in ISES Solar World Congress 2001 & 2003 Proceedings. 2003.

[81] Ait Lahoussine Ouali, H., et al., Optimization and techno-economic appraisal of parabolic trough solar power plant under different scenarios: a case study of Morocco. Energies, 2022. 15(22): p. 8485.

[82] Liu, C., et al., A wind power plant with thermal energy storage for improving the utilization of wind energy. Energies, 2017. 10(12): p. 2126.

[83] Chatzivasileiadi, A., E. Ampatzi, and I. Knight, Characteristics of electrical energy storage technologies and their applications in buildings. Renewable and Sustainable Energy Reviews, 2013. 25: p. 814-830.

[84] Niveditha, N. and M.R. Singaravel, Optimal sizing of hybrid PV–Wind–Battery storage system for Net Zero Energy Buildings to reduce grid burden. Applied Energy, 2022. 324: p. 119713.

[85] Yaïci, W., et al. Hybrid Renewable Energy Systems with Hydrogen and Battery Storage Options for Stand-Alone Residential Building Application in Canada. in 2022 11th International Conference on Renewable Energy Research and Application (ICRERA). 2022. IEEE.

[86] Yang, J., et al., Thermodynamic analysis and optimization of a solar organic Rankine cycle operating with stable output. Energy Conversion and Management, 2019. 187: p. 459-471.

[87] Desai, N.B. and S. Bandyopadhyay, Thermo-economic comparisons between solar steam Rankine and organic Rankine cycles. Applied Thermal Engineering, 2016. 105: p. 862-875.

[88] Spayde, E., P.J. Mago, and H. Cho, Performance evaluation of a solar-powered regenerative organic Rankine cycle in different climate conditions. Energies, 2017. 10(1): p. 94.

[89] Li, J., et al., Thermodynamic performance analyses and optimization of subcritical and transcritical organic Rankine cycles using R1234ze (E) for 100–200° C heat sources. Energy Conversion and Management, 2017. 149: p. 140-154.

[90] Freeman, J., et al., A small-scale solar organic Rankine cycle combined heat and power system with integrated thermal energy storage. Applied thermal engineering, 2017. 127: p. 1543-1554.

[91] Clerc, M., Particle swarm optimization. Vol. 93. 2010: John Wiley & Sons.

[92] Kalatehjari, R., et al., The contribution of particle swarm optimization to three-dimensional slope stability analysis. The Scientific World Journal, 2014. 2014.

[93] Marocco, P., et al., A study of the techno-economic feasibility of H2-based energy storage systems in remote areas. Energy Conversion and Management, 2020. 211: p. 112768.